Physically-Feasible Reactive Synthesis for Terrain-Adaptive Locomotion

Anonymous Author(s)

***Abstract*—We propose an integrated planning framework for quadrupedal locomotion over dynamically changing, unforeseen terrains. Existing approaches either rely on heuristics for instantaneous foothold selection–compromising safety and versatility–or solve expensive trajectory optimization problems with complex terrain features and long time horizons. In contrast, our framework leverages reactive synthesis to generate correct-by-construction controllers at the symbolic level, and mixed-integer convex programming (MICP) for dynamic and physically feasible footstep planning for each symbolic transition. We use a high-level manager to reduce the large state space in synthesis by incorporating local environment information, improving synthesis scalability. To handle specifications that cannot be met due to dynamic infeasibility, and to minimize costly MICP solves, we leverage a symbolic repair process to generate only necessary symbolic transitions. During online execution, re-running the MICP with real-world terrain data, along with runtime symbolic repair, bridges the gap between offline synthesis and online execution. Through extensive simulation and hardware experiments, we demonstrate our framework's capabilities to discover missing locomotion skills and react promptly in safety-critical environments, such as scattered stepping stones and rebars.**

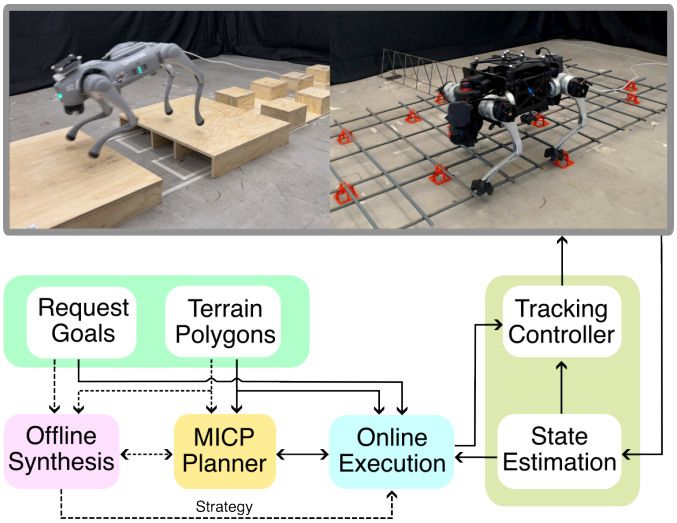

Fig. 1. System architecture overview. The solid lines indicate online communication, while dashed lines represent offline processes. The request goals in the offline phase are user-defined, while those in the online phase are provided by a global planner based on the global goal.

I. Introduction

Terrain-adaptive locomotion is crucial for enhancing the traversing capabilities of legged robots and advancing beyond blind locomotion [1]–[3]. Existing approaches that enable terrain-adaptive and dynamic locomotion focus on instantaneous foothold adaptation [4], [5] around a nominal reference trajectory. To further enhance the traversability, non-fixed gait pattern has been studied. In [6]–[8], jumping motions are generated offline and triggered through heuristics when facing an obstacle. In [9], [10], the switch between normal walking and jumping is either embedded inside a reduced-order model during sampling [9] or decided by a pre-trained feasibility classifier [10]. However, formal guarantees on locomotion safety [11], [12], considering the robot's physical capabilities for traversing challenging terrains, are rarely explored—despite their importance in safety-critical scenarios like hazardous debris and construction sites as shown in Fig. 1.

Mixed-integer program (MIP)-based approaches [13], [14] treat both the contact state and the contact plane selection for each leg at each timestep as binary variables, and directly address the interplay between terrain segments and robot kinematics and dynamics [15]. By relaxing the dynamics and constraints, a global certificate for the approximated convex problem (MICP) exists upon convergence [16], providing an ideal means to formally determine the locomotion feasibility. However, long time horizon and complex features of surrounding terrains significantly increase the computational burden for MIP-based methods, preventing efficient online deployment. Simplifications have been made to enhance speed, *e.g.*, assuming predetermined contact sequences [17], [18] and timing [19]–[21], or fixing the number of footsteps [22], but still face computational challenges in complicated scenarios with a large number of terrain segments.

To reduce the complexity of navigating challenging terrains, one approach is to break down global, long-horizon tasks into dynamically evolving, robot-centric local environments with intermediate waypoints [4]. However, the corresponding MIP remains computationally expensive because it must consider all surrounding terrains. To address this, we discretize the local environment and restrict the MIP formulation to solving only individual discrete transitions. To efficiently compose these discrete transitions with formal correctness guarantees, we employ Linear Temporal Logic (LTL)-based reactive synthesis [23] to generate a correct-by-construction robot strategy that guides the composition of MIP-based transitions toward the intermediate goals.

In this paper, we combine reactive synthesis and MIP-based approaches to safely and promptly react to dynamically changing environments. We abstract the continuous robot states and local environments into symbolic states, enabling high-level robot actions on the fly toward challenging terrains such as obstacles and large gaps, as shown in Fig. 1. We

then solve a MICP to provide a physical feasibility certificate for each symbolic transition. This integrated framework not only bridges the gap between high-level abstraction and low-level physical capabilities but also alleviates the computational burden of MICP. Guided by the synthesis-based symbolic planner, each MICP can consider shorter time horizons and fewer terrain features than traditionally solving a single, long-horizon MICP problem. Another noteworthy feature of our planning framework is its two-stage hierarchy. In the offline synthesis phase, we leverage relatively expensive gait-free MICPs that optimize both contact state and foothold selection to generate the necessary locomotion gaits for symbolic transitions. In the online execution phase, we use efficient gait-fixed MICPs with predefined gaits to produce dynamically feasible motions and footholds on the fly. Moreover, the proposed approach is flexible in that it can be used to follow commands from a global/higher-level planner [9], [10], [24]–[27] or from a user, and can incorporate additional locomotion behavior as needed.

Our offline synthesis module tackles two key scalability challenges. First, our task specification has a prohibitively large state space since it needs to encode the surrounding terrain states. Since our synthesis algorithm has exponential time complexity in the number of variables [23], it is inefficient and impractical to directly synthesize a controller for the full specification. To tackle this challenge, we leverage an observation that the robot can continuously reason about its local environment where the terrains and an intermediate goal remain unchanged. Thus, we propose a high-level manager that fixes the terrain and goal information, only keeps the skills needed for the current terrains, and updates them as the robot moves in the environment. In our experiment, the manager reduces the number of variables by $80.9 - 90.1\%$ depending on the number of cells and terrain types, relieving the computation burden of synthesis.

Our second scalability challenge is that, while the size of the MICP for our physical feasibility certificate is much smaller than the pure MIP approach, solving gait-free MICP is still computationally expensive. To mitigate this problem, we leverage a symbolic repair approach [28] to automatically suggest only the missing, yet necessary, symbolic transitions, and only solve MICP for them. In this way, we avoid enumerating and solving the costly MICP for all possible symbolic transitions. In our experiments, the symbolic repair reduces the number of expensive MICP solves by $71.7-97.6\%$ depending on the terrains, compared with exhaustively iterating over all possible symbolic transitions, ensuring that we only perform the costly gait-free MICP to generate new locomotion gaits when necessary.

Our online execution module also tackles two key challenges. First, discrepancies in size and shape between offline-checked terrains and real-world ones can lead to mismatches between the desired symbolic transitions and the robot's actual physical capabilities. Second, encountering new terrains or intermediate goals not considered in the offline phase may also make symbolic specifications unrealizable, as the unforeseen scenarios are not handled during the offline phase. As such, our online execution module executes each symbolic transition by solving an online MICP with real-world terrain data and prior locomotion gaits to generate a new nominal trajectory. If a symbolic transition is no longer possible or the current terrains and goal were not considered offline, we perform runtime repair, as done in [29], to generate new robot skills and synthesize an updated robot strategy, allowing continuous traversal on unexpected terrains.

The primary contributions of this paper are as follows:

- We propose an integrated planning framework that combines reactive synthesis with MICP for terrain-adaptive locomotion. Compared to pure MIP approaches, our method reduces computational burden via symbolic guidance and a two-stage hierarchy.
- During offline synthesis, we overcome scalability challenges by leveraging a high-level manager to reduce the size of the specifications based on local environment information, and symbolic repair to minimize the number of calls to the costly gait-free MICP, enabling efficient synthesis of terrain-adaptive locomotion strategies.
- During online execution, we address the disparity between offline synthesis and real-world terrain conditions at both the physical and symbolic levels. Our approach leverages an online MICP solver along with an online symbolic repair process to account for real-world terrain discrepancies and newly encountered conditions, enhancing robustness and motion feasibility at runtime.

We validate the entire framework through extensive simulation and hardware experiments, benchmarking it against both a heuristics-based footstep planner and a pure MIP planner. Code and experimental videos are available at https://synthesis-micp.github.io/.

II. Related Work

A. Hierarchical Planning for Terrain-Adaptive Locomotion

Planning for terrain-adaptive locomotion can be boiled down into solving contact sequence and timing (equivalently gait), location (equivalently foothold), and robot motion (e.g., Center of Mass (CoM) or base pose), given the chosen kinematics/dynamics model and the perceived terrain information. Hierarchical approaches first separately or simultaneously address part of the above problems and then solve for the rest, which allows for higher computational efficiency. Kinematic footstep planning focuses on the first two problems, neglecting the robot dynamics through graph-based approaches [4], [30]–[34] or optimization-based approaches [15], [20], [35]. Although non-fixed gait/contact plans can be generated for very rough terrains [36]–[38], conservative quasi-static motions are generated for challenging terrains due to the kinematic simplification during footstep planning.

Given the recent advances in optimization-based approaches, notably Model Predictive Control (MPC), another focus of the literature is on the local foothold adaptation and the integration of robot dynamics for dynamic locomotion. Instantaneous foothold adaptation around a nominal location,

with a fixed and cyclic gait, is performed based on heuristic search [7], [39], [40] or learning approaches [41]–[44]. In [5], [45], [46], the base pose and foothold are optimized jointly, demonstrating impressive terrain traversing capabilities on rough terrains.

However, the above dynamic locomotion works consider a fixed gait pattern that usually prohibits achieving versatile behaviors, such as jumping. In [6]–[8], jumping motions are generated offline and triggered through heuristics. In [9], [10], [25], RRT-Connect is used for rapid kino-dynamic locomotion planning, and the switch between normal walking and jumping is either embedded inside a reduced-order model during sampling [9] or decided by a pre-trained feasibility classifier [10]. Beyond limited gait modes, other works focus on online gait planning and/or foothold selection and deploy MPC to track the plan, which can be further categorized into model-free [47]–[51] and model-based methods [52]–[54].

B. Simultaneous Planning via Optimization

Planning for terrain-adaptive locomotion problem can also be formulated as a combinatorial optimization problem that simultaneously optimizes for gait, foothold, and robot dynamics. One approach is to incorporate rigid [55] or smoothed [56] complementarity constraints, which accurately model the physical contact interaction behavior but remains computationally inefficient due to the non-smoothness and highly nonlinearity. Promising online contact-implicit MPC results are reported in [57], [58] but still limited to low-dimensional system or static environment.

Another way of encoding discrete contact decisions is to treat both the contact state and the contact plane selection for each leg at each timestep as binary variables [13], [14], [59]. The underlying problem can be formulated as Mixed Integer Program (MIP). Convex approximations of nonlinear dynamics, usually centroidal dynamics, and constraints are typically required to transform the MIP into a more tractable Mixed Integer Convex Program (MICP), albeit with an increased number of binary variables. A global certificate for the approximated convex problem exists upon convergence [16], providing an ideal means to determine the feasibility in our proposed method. To relieve the computational burden due to the introduction of many binary variables, the works of [17], [19], [21] assume the contact sequence and timing are chosen *a prior*, and only optimize the contact plane selection. Aceituno-Cabezas et al. [22] optimize the contact sequence within a certain gait cycle that fixes the number of footsteps. However, it is inevitable that the problem complexity grows exponentially when the number of discrete contact options increases along with the time horizon and terrain features. Our work aims to alleviate computational burden through a two-stage approach. In the offline phase, expensive MICPs that optimize both contact state and foothold selection are solved to generate necessary locomotion gaits. In the online phase, efficient MICPs with adaptive and predefined gaits are used to produce dynamically feasible motions and footholds. Additionally, guided by a synthesis-based task planner, each MICP in our work considers shorter time horizons and fewer terrain features compared to solving a single large MICP problem.

C. Task and Motion Planning for Contact-Rich Planning

Task and Motion Planning (TAMP) formally defines symbolic-level tasks and searches through a graph of predefined motion primitives that enable feasible symbolic transitions [60]. For more complex physical contact resoning, Toussaint et al. propose Logic Geometric Programming (LGP) [61] and embed the high-level logic representation into the low-level motion planner, demonstrating contact-rich tool-use behaviors [62] after defining abundant action primitives. Building on this, a broader range of motions has been showcased, including versatile manipulation [63], [64] and loco-manipulation tasks [65]. In a similar vein, works such as [66]–[73] integrate graph-search or sampling-based methods with optimization-based approaches in a holistic manner, abstracting contact modes within a discrete domain. However, the combinatorial nature of these problems often leads to poor scalability due to the explosion of contact modes. Deploying such approaches online in dynamic environments remains an open challenge. From a different perspective, we abstract a smaller set of task-level contact modes as locomotion gaits over a specific time horizon and distance, allowing the MICP to solve for details such as contact locations and robot motion during execution. This shifts the focus to selecting locomotion gaits within a local environment while ensuring safety and completeness through synthesis-based approaches.

Unlike LGP that solves an integrated TAMP problem, synthesis-based approaches using Linear Temporal Logic (LTL) operate primarily at the task level, emphasizing safety and completeness guarantees within the task domain [74]. These methods typically synthesize a sequence of task-level actions, which are then executed by a motion planner. Recently, LTL has been applied to safe locomotion tasks, employing distinct task-level abstractions on topological maps of terrain [75]–[77] or locomotion keyframes for reduced-order models [11], [12], [78]. Reactive synthesis [79], widely applied to mobile robots [80], has been employed to enable prompt decision-making in response to more complex environments [12] or external perturbations [78]. Notably, Zhao et al. [11] formulate the terrain-adaptive locomotion problem as a sequential decision-making task, selecting appropriate locomotion modes with predefined contact and locomotion keyframes to accommodate dynamically changing terrains. However, the locomotion mode selection is explicitly encoded in the LTL specification using expert knowledge, lacking a physically feasibility guarantee. In this work, we aim to combine the strengths of reactive synthesis and MICP, utilizing the global certificate of MICP as a feasibility checker for terrain-adaptive locomotion.

D. Physically-Feasible Reactive Synthesis

While reactive synthesis can promptly and safely respond to dynamic environments, it typically does not assess physical

feasibility when being deployed on complex robotic systems. To bridge the gap between discrete abstraction and continuous system dynamics, various strategies have been proposed. Studies in [81], [82] focus on automatically synthesizing controllers in the continuous domain based on high-level specifications. Another approach involves incorporating dynamics directly into the reactive synthesis process by abstracting physical systems, including nonlinear [83], switched [84], and hybrid systems [85] with manageable model complexity. However, for legged robots with multiple contacts navigating dynamic terrains, these physically feasible reactive synthesis approaches remain computationally intractable.

Recent efforts [28], [86] focus on symbolic repair for unrealizable task specifications, defining symbolic skills with preconditions and postconditions, similar to TAMP, to identify missing skills that make the specification realizable. These works introduce iterative feasibility checks based on symbolic repair suggestions, emphasizing alignment between symbolic task specifications and physical reality. Building upon this, Meng et al. [29] extends this type of approach to online symbolic repair. Inspired by these works, we adopt a similar mechanism for terrain-adaptive locomotion. Specifically, we abstract the robot and terrain states in a local environment and define physically feasible skills by solving MICP. To address scalability issues arising from complex terrain features, we employ a high-level manager to decompose the problem into smaller subproblems, enabling faster repair and synthesis. In addition, we leverage symbolic repair to identify missing but necessary skills, reducing the need for frequent calls to the computationally expensive gait-free MICP.

III. Preliminaries

Consider a robot equipped with sensors navigating an environment toward a designated global goal $g_{\text{global}} \in \mathbb{R}^2$. This task can be decomposed into a series of local navigation tasks, where the robot moves toward intermediate, local request goals $\mathcal{G}_{\text{local}}$ as guided by a global planner, given surrounding segmented terrain polygons $\mathcal{P}$. We illustrate an example of this local task.

Example 1. *Consider a 2D grid world with nine cells (in yellow) in Fig. 2. The robot is required to move from an initial cell (e.g. the center cell) to a desired goal cell indicated by the star. Each cell is assigned a terrain type, such as Dense or Sparse stepping stones.*

A. Abstractions

Given a set of terrain polygons $\mathcal{P}$, e.g., in Fig. 2(a), we abstract them into a 2D grid of size $n \times m$. For each dimension, we denote each location in that dimension with a symbol, resulting in two sets $\mathcal{X} := \{x_0, \dots, x_{n-1}\}$ and $\mathcal{Y} := \{y_0, \dots, y_{m-1}\}$. We define a set of atomic propositions AP, partitioned into sets of inputs $\mathcal{I}$ and outputs $\mathcal{O}$, to describe the symbolic world states and robot actions. The inputs $\mathcal{I}$ consist of the robot inputs $\mathcal{I}_{\text{robot}}$, the request inputs $\mathcal{I}_{\text{req}}$, and the terrain inputs $\mathcal{I}_{\text{terrain}}$ ($\mathcal{I} = \mathcal{I}_{\text{robot}} \cup \mathcal{I}_{\text{req}} \cup \mathcal{I}_{\text{terrain}}$). The robot inputs $\mathcal{I}_{\text{robot}} := \{\pi_x \mid x \in \mathcal{X}\} \cup \{\pi_y \mid y \in \mathcal{Y}\}$ are used to abstract the robot position, the request inputs $\mathcal{I}_{\text{req}} := \{\pi_x^{\text{req}} \mid x \in \mathcal{X}\} \cup \{\pi_y^{\text{req}} \mid y \in \mathcal{Y}\}$ are used to abstract the requested goal cells, and the terrain inputs $\mathcal{I}_{\text{terrain}} := \{n_x^y \mid x \in \mathcal{X}, y \in \mathcal{Y}\}$ describe the terrain type of the grid cells. The robot state can be extended to incorporate orientation information, such as the floating base's yaw angle, as demonstrated in Sec. IX-F. We then consider a finite set of size n_t of terrain types, defined based on their physical characteristics. For $z \in \mathbb{N}$, we denote $[z] := \{0, \dots, z-1\}$. We note that terrain inputs $n_x^y \in \mathcal{I}_{\text{terrain}}$ are integer variables belonging to $[n_t]$, and we translate them into a set of Boolean propositions, as done in [87]. An input state $\sigma_{\mathcal{I}}$ is a value assignment function $\sigma_{\mathcal{I}} : \mathcal{I} \to \{\texttt{True}, \texttt{False}\} \cup [n_t]$. Since the robot can only be in one cell at a time, and the goal is a single cell, we require that exactly one π_x, one π_y, one π_x^{req}, and one π_y^{req} be $\texttt{True}$, for each input state. The robot states $\sigma_{\text{robot}} : \mathcal{I}_{\text{robot}} \to \{\texttt{True}, \texttt{False}\}$, request states $\sigma_{\text{req}} : \mathcal{I}_{\text{req}} \to \{\texttt{True}, \texttt{False}\}$, and terrain states $\sigma_{\text{terrain}} : \mathcal{I}_{\text{terrain}} \to [n_t]$ are the projections of $\sigma_{\mathcal{I}}$ on $\mathcal{I}_{\text{robot}}$, $\mathcal{I}_{\text{req}}$, and $\mathcal{I}_{\text{terrain}}$, respectively. We denote the sets of input states as $\Sigma_{\mathcal{I}}$, robot states as Σ_{robot}, request states as Σ_{req}, and terrain states as Σ_{terrain}.

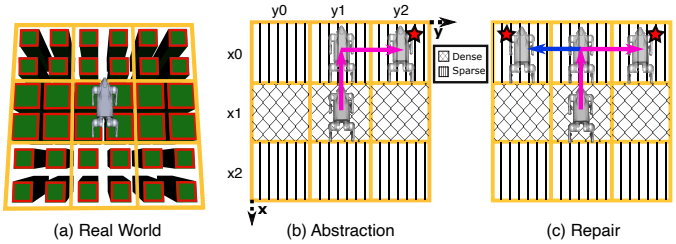

Fig. 2. Terrain abstraction and skill definition. (a) Top-down view of the real-world terrain before abstraction. The red polygons denote the segmented terrain polygons. (b) Abstraction of the terrain and robot's skills (pink) moving from one location to another. (c) Repair process to find a new skill (blue).

We use a grounding function to describe the physical meaning of input states. Consider a physical state space $\mathcal{Z} \subseteq \mathbb{R}^n$ that represents the physical world, including the robot's position, orientation, and terrain properties. The grounding function $\text{G} : \Sigma_{\mathcal{I}} \to 2^{\mathcal{Z}}$ maps each input state $\sigma_{\mathcal{I}}$ to a set of physical states in $\mathcal{Z}$. For robot states $\sigma_{\text{robot}} \in \Sigma_{\text{robot}}$, we define $\text{G}(\sigma_{\text{robot}}) := \{z \in \mathcal{Z} \mid \exists \pi_x, \pi_y \in \mathcal{I}_{\text{robot}}.\sigma_{\text{robot}}(\pi_x) \wedge \sigma_{\text{robot}}(\pi_y) \wedge \text{robot\_pose}(z) \in \text{cell}(x, y)\}$. Similarly, for request states $\sigma_{\text{req}} \in \Sigma_{\text{req}}$, we define $\text{G}(\sigma_{\text{req}}) := \{z \in \mathcal{Z} \mid \exists \pi_x^{\text{req}}, \pi_y^{\text{req}} \in \mathcal{I}_{\text{req}}.\sigma_{\text{req}}(\pi_x^{\text{req}}) \wedge \sigma_{\text{req}}(\pi_y^{\text{req}}) \wedge \text{request\_goal}(z) \in \text{cell}(x, y)\}$. For terrain states $\sigma_{\text{terrain}} \in \Sigma_{\text{terrain}}$, we define $\text{G}(\sigma_{\text{terrain}})$ to be the set of physical states whose abstracted terrain types are indicated by σ_{terrain}. For an input state $\sigma_{\mathcal{I}} \in \Sigma_{\mathcal{I}}$ whose projections are σ_{robot}, σ_{req}, and σ_{terrain}, $\text{G}(\sigma_{\mathcal{I}}) := \text{G}(\sigma_{\text{robot}}) \cap \text{G}(\sigma_{\text{req}}) \cap \text{G}(\sigma_{\text{terrain}})$. Lastly, we use an inverse grounding function $\text{G}^{-1} : \mathcal{Z} \to \Sigma_{\mathcal{I}}$ to map a physical state $z \in \mathcal{Z}$ to its corresponding input state.

In Example 1, the inputs are $\mathcal{I}_{\text{robot}} := \{\pi_{x_0}, \pi_{x_1}, \pi_{x_2}, \pi_{y_0}, \pi_{y_1}, \pi_{y_2}\}$, $\mathcal{I}_{\text{req}} := \{\pi^{\text{req}} \mid \pi \in \mathcal{I}_{\text{robot}}\}$, and $\mathcal{I}_{\text{terrain}} := \{n_{x_i}^{y_j} \mid i, j \in \{0, 1, 2\}\}$ where $n_{x_i}^{y_j} = 1$ if the terrain type of the grid cell (x_i, y_j) is Dense, and $n_{x_i}^{y_j} = 0$

if it is Sparse. The input state in Fig. 2(b) is $\sigma_{\mathcal{I}} : \pi_{x_1} \mapsto \texttt{True}, \pi_{y_1} \mapsto \texttt{True}, \pi^{\text{req}}_{x_0} \mapsto \texttt{True}, \pi^{\text{req}}_{y_2} \mapsto \texttt{True}, n^{y_j}_{x_1} \mapsto 1$ for $j \in \{0, 1, 2\}$. In this paper, we omit the Boolean propositions that are `False` and integer propositions whose values are 0 in the input states for space.

The outputs $\mathcal{O}$ represent the skills that allow the robot to transit among grid cells, given their corresponding terrain states. A skill $o \in \mathcal{O}$ consists of sets of preconditions $\Sigma^{\text{pre}}_o \subseteq \Sigma_{\text{robot}} \times \Sigma_{\text{terrain}}$, from which the skill is allowed to execute, and postconditions $\Sigma^{\text{post}}_o \subseteq \Sigma_{\text{robot}}$, the resulting grid cell after executing the skill. In Example 1, the skill o_0 moves the robot from the middle to the upper terrain grid cell (Fig. 2b). The precondition of o_0 is $\Sigma^{\text{pre}}_{o_0} = \{(\sigma_{\text{robot}}, \sigma_{\text{terrain}}) : \pi_{x_1} \mapsto \texttt{True}, \pi_{y_1} \mapsto \texttt{True}, n^{y_0}_{x_1} \mapsto 1, n^{y_1}_{x_1} \mapsto 1, n^{y_2}_{x_1} \mapsto 1\}$, The postcondition is $\Sigma^{\text{post}}_{o_0} = \{\sigma_{\text{robot}} : \pi_{x_0} \mapsto \texttt{True}, \pi_{y_1} \mapsto \texttt{True}\}$. In addition, each skill consists of a continuous-level locomotion gait, e.g. a one-second trotting gait L, that physically implements the symbolic transition (Sec. VI-A).

B. Specifications

We use the Generalized Reactivity(1) (GR(1)) fragment of linear temporal logic (LTL) [23] to encode task specifications. LTL specifications φ follow the grammar $\varphi := \pi \mid \neg\varphi \mid \varphi \wedge \varphi \mid \bigcirc\varphi \mid \square\varphi \mid \lozenge\varphi$, where $\pi \in AP$ is an atomic proposition, $\neg$ "not" and $\wedge$ "and" are Boolean operators, and $\bigcirc$ "next", $\square$ "always", and $\lozenge$ "eventually" are temporal operators. We refer the readers to [88] for a detailed description of LTL.

GR(1) specifications are expressed in the form of $\varphi = \varphi_{\text{e}} \rightarrow \varphi_{\text{s}}$, where $\varphi_{\text{e}} = \varphi^{\text{i}}_{\text{e}} \wedge \varphi^{\text{t}}_{\text{e}} \wedge \varphi^{\text{g}}_{\text{e}}$ is the assumptions on the behaviors of the possibly adversarial environment, and $\varphi_{\text{s}} = \varphi^{\text{i}}_{\text{s}} \wedge \varphi^{\text{t}}_{\text{s}} \wedge \varphi^{\text{g}}_{\text{s}}$ represents the guarantee of the desired robot's behaviors. For $\alpha \in \{e, s\}$, $\varphi^{\text{i}}_{\alpha}, \varphi^{\text{t}}_{\alpha}, \varphi^{\text{g}}_{\alpha}$ characterize the initial conditions, safety constraints, and liveness conditions, respectively. For symbolic repair (see Sec. VI-C), we divide safety constraints $(\varphi^{\text{t}}_{\text{e}}, \varphi^{\text{t}}_{\text{s}})$ into skill constraints $(\varphi^{\text{t,skill}}_{\text{e}}, \varphi^{\text{t,skill}}_{\text{s}})$ and hard constraints $(\varphi^{\text{t,hard}}_{\text{e}}, \varphi^{\text{t,hard}}_{\text{s}})$, i.e., for $\alpha \in \{e, s\}$, $\varphi^{\text{t}}_{\alpha} = \varphi^{\text{t,skill}}_{\alpha} \wedge \varphi^{\text{t,hard}}_{\alpha}$. The skill constraints encode the pre and postcondition of skills (see Sec. VI-B) and can be modified by repair, while repair cannot modify the hard constraints.

In practice, the GR(1) specifications are large in size due to the necessity of encoding terrain and task information. Since the exact current terrain and request state information is available at runtime, we can generate a shorter and more efficient version of the specification via *partial evaluation*, which substitutes a subset of the Boolean propositions with their truth values to reduce the state space.

Definition 1. Given an LTL formula φ and two subsets $S^{\texttt{True}}, S^{\texttt{False}} \subseteq AP$, $S^{\texttt{True}} \cap S^{\texttt{False}} = \emptyset$, we define the *partial evaluation* of φ over $S^{\texttt{True}}, S^{\texttt{False}}$, as $\varphi[S^{\texttt{True}}, S^{\texttt{False}}]$, where we substitute propositions $\pi \in AP$ in φ with `True` if $\pi \in S^{\texttt{True}}$ and with `False` if $\pi \in S^{\texttt{False}}$.

IV. Problem Statement

Problem 1. Given (i) a global goal g_{global}, (ii) a set of possible local request goals $\mathcal{G}_{\text{local}}$ (iii) a set of predefined terrain polygons $\mathcal{P}_{\text{pre}}$ from user's prior knowledge, and (iv) a set of online terrain polygons $\mathcal{P}_{\text{on}}$ perceived during execution that may differ from the predefined ones, (v) a set of predefined locomotion gaits $\mathcal{L}$; generate controls that enable the robot to navigate the environment and reach the goal.

V. Approach Summary

To efficiently solve Problem 1, we manage complexity at both symbolic and physical levels. At the symbolic level, we leverage reactive synthesis to decompose the local navigation problem into manageable subproblems whose solutions can be reused by synthesis for different scenarios. Each subproblem corresponds to finding controls for a short-horizon symbolic transition and is solved via a MICP to provide physical feasibility certificates of the transition. As shown in Fig. 1, our framework consists of offline synthesis (Sec.VI), online execution (Sec.VII), and low-level tracking control (Sec.VIII). During the offline phase, we generate a set of potentially useful skills and corresponding locomotion gaits based on predefined terrain states and goals, while leveraging symbolic repair to find missing yet necessary symbolic transitions. At runtime, we leverage runtime repair to identify new symbolic transitions necessary for unforeseen terrain configurations or intermediate request goals.

VI. Offline Synthesis

The offline synthesis module generates a strategy that enables the robot to reach local request goals over predefined terrain states. As shown in Fig. 3(a), this module takes in a set of local request goals $\mathcal{G}_{\text{local}}$ and a set of possible terrain polygons $\mathcal{P}_{\text{pre}}$ from prior knowledge of the workspace. In addition, the user provides a set of locomotion gaits $\mathcal{L}$. We first leverage the inverse grounding function G^{-1} to discretize the local environment, obtain a set of possible request states $\Sigma^{\text{poss}}_{\text{req}} \subseteq \Sigma_{\text{req}}$ from the local request goals, and characterize the predefined set of terrain polygons into a set of possible terrain states $\Sigma^{\text{poss}}_{\text{terrain}} \subseteq \Sigma_{\text{terrain}}$. Next, we solve a gait-fixed MICP problem to determine the feasibility of each potential skill given the locomotion gaits (Sec. VI-A), and then encode all feasible transitions as skills in a specification (Sec. VI-B). Next, we use a high-level manager to generate partial evaluations of the encoded specifications for efficient synthesis. If any partial evaluation is unrealizable, we use a repair process to suggest new robot skills and a gait-free MICP to check the feasibility of the suggested skills, eventually making the specification realizable (Sec. VI-C).

A. Locomotion Gait and Feasibility Checking via MICP

We assume each locomotion gait L comes with a contact sequence $\mathcal{G}$ and corresponding time durations T. Therefore, we define the locomotion gait as $L = \mathcal{M}(\mathcal{G}, T)$. Each skill is assumed to have a unique locomotion gait to determine how the robot moves at the continuous level. As shown in Fig. 3(a), since all the possible request states $\Sigma^{\text{poss}}_{\text{req}}$ and terrain states $\Sigma^{\text{poss}}_{\text{terrain}}$ are given during the offline phase, it is straightforward to first identify all the potential skills at the symbolic level that allow the robots to move freely in all possible local

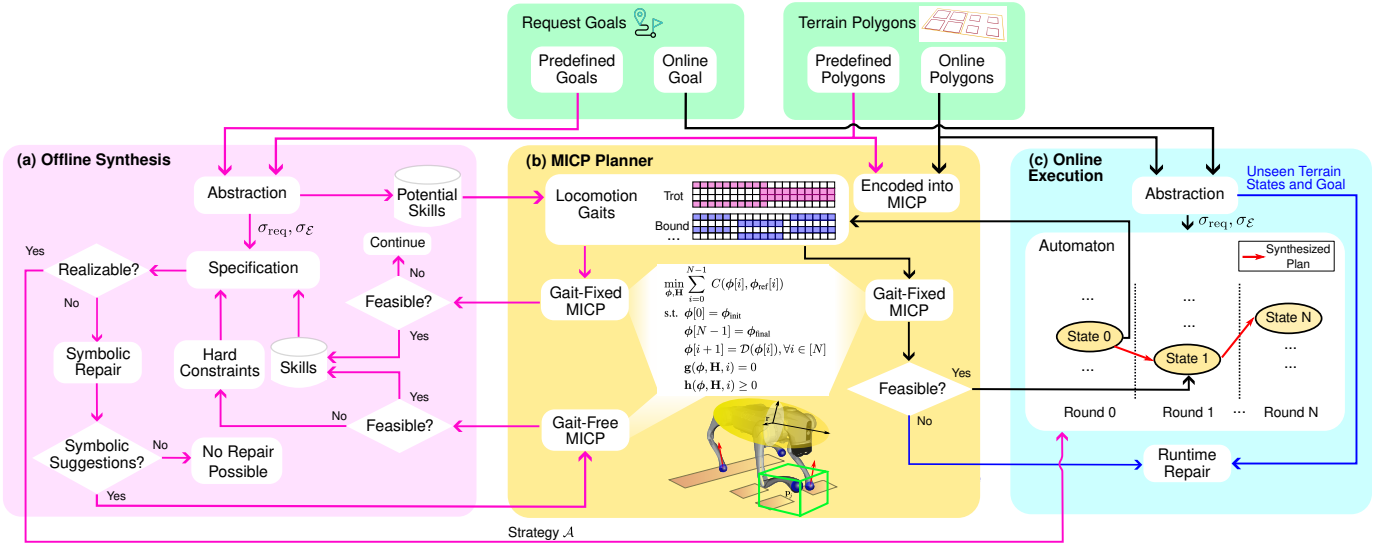

Fig. 3. System overview. During offline synthesis (pink arrows), an initial set of locomotion gaits is provided, and symbolic skills are iteratively generated by solving the MICP. When the task specifications are unrealizable, a symbolic repair is triggered to seek missing skills. During the online execution (black arrows), MICP is solved again taking online terrain segments and the symbolic state only advances when a solution is found. A runtime repair (blue arrows) is initiated if a solving failure occurs, or an unseen terrain or request goal is encountered.

environments. Each of them is evaluated by a gait-fixed MICP using the provided locomotion gaits. In most examples shown in this paper, we assume the robot is only allowed to move horizontally and vertically by one cell and we show diagonal movements and heading angle change in Sec. IX-F.

Then the next critical step is to find whether there exists a locomotion gait for each skill to be physically feasible. We leverage mixed-integer convex programming (MICP) to check the physical feasibility given a set of predefined locomotion gaits, and only use the feasible one as robot skills to synthesize robot strategies. The MICP problem takes in the centroidal states $\mathcal{I}_{\text{robot}}$ from the precondition and postcondition of the skill as its initial and final conditions, which are located at the center of each abstracted cell. A set of homogeneous, predefined terrain polygons are considered in the MICP as steppable regions corresponding to the terrain states $\mathcal{I}_{\text{terrain}}$ involved in the precondition. Lastly, the contact information $\mathcal{G}$ and T is provided by the selected locomotion gait L. Fig. 4 shows the maneuver of the quadruped robot Go2 after solving the MICP problem corresponding to skill a_0 in Example 1 with a one-second trotting locomotion gait. The generic MICP problem considered in this work can formulated as:

$$\min_{\boldsymbol{\phi},\mathbf{H}} \sum_{i=0}^{N-1} C(\boldsymbol{\phi}[i], \boldsymbol{\phi}_{\text{ref}}[i])$$

$$\text{s.t. } \boldsymbol{\phi}[0] = \boldsymbol{\phi}_{\text{init}} \tag{1a}$$

$$\boldsymbol{\phi}[N-1] = \boldsymbol{\phi}_{\text{final}} \tag{1b}$$

$$\boldsymbol{\phi}[i+1] = \mathcal{D}(\boldsymbol{\phi}[i]), \forall i \in [N] \tag{1c}$$

$$\mathbf{g}(\boldsymbol{\phi}, \mathbf{H}, i) = 0 \tag{1d}$$

$$\mathbf{h}(\boldsymbol{\phi}, \mathbf{H}, i) \geq 0 \tag{1e}$$

where the decision variables $\boldsymbol{\phi}$ denote the continuous variables

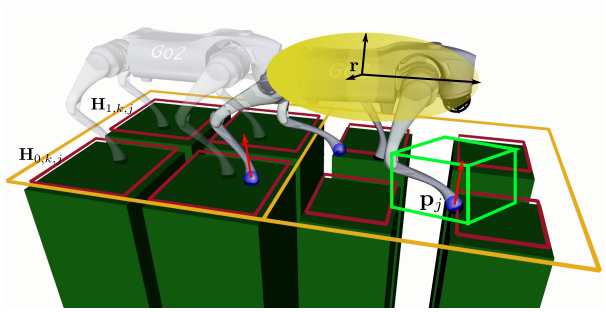

Fig. 4. Demonstration of decision variables and polygons when solving MICP for skill a_0 in Example 1 using a trotting locomotion gait.

and $\mathbf{H}$ indicate the binary variables across the entire N timesteps. For any natural number $n \in \mathbb{N}$, we denote the set $\{0, \ldots, n-1\}$ as $[n]$. The general equality constraints $\mathbf{g}(\cdot)$ and inequality constraints $\mathbf{h}(\cdot)$ are incorporated and activated at certain time stamp i. The cost function depends on both the continuous variables $\boldsymbol{\phi}$ and a reference trajectory $\boldsymbol{\phi}_{\text{ref}}$.

The reference base position and angular trajectories are generated by linearly interpolating between the initial and final conditions. For scenarios with significant elevation changes, such as jumping onto higher terrain, an additional middle keyframe is introduced for the pitch angle to calculate the slope angle between the initial and final poses. The final reference pitch trajectory is then created by evenly interpolating between the initial, middle, and final poses. The reference EE trajectory relative to the base frame ${}^{\mathcal{B}}\mathbf{p}_j^{\text{ref}}$ remains constant and moves in sync with the reference base trajectory.

Given a specific locomotion gait, we first introduce the gait-fixed MICP formulation:

TABLE I
TRACKING COST WEIGHTS

Cost Term	Weights
$\mathbf{r} - \mathbf{r}_{\text{ref}}$	(1000.0, 1000.0, 1000.0)
$\boldsymbol{\theta} - \boldsymbol{\theta}_{\text{ref}}$	(1000.0, 1000.0, 1000.0)
$\mathbf{p}_j - \mathbf{p}_j^{\text{ref}}$	(1000.0, 1000.0, 1000.0)
$\ddot{\mathbf{r}}$	(10.0, 10.0, 10.0)
$\ddot{\boldsymbol{\theta}}$	(10.0, 10.0, 10.0)
$\ddot{\mathbf{p}}_j$	(0.5, 0.5, 0.5)
$\mathbf{f}_j$	(0.1, 0.1, 0.1)

1) Continuous Decision Variables: The continuous decision variables ϕ include base position $\mathbf{r}$, velocity $\dot{\mathbf{r}}$, acceleration $\ddot{\mathbf{r}}$, orientation $\boldsymbol{\theta}$ parameterized by Euler angle and its first and second-order derivatives $\dot{\boldsymbol{\theta}}, \ddot{\boldsymbol{\theta}}$, individual end-effector (EE) position $\mathbf{p}_j$, velocity $\dot{\mathbf{p}}_j$, and acceleration $\ddot{\mathbf{p}}_j$, and individual contact force $\mathbf{f}_j$ for the foot j with $j \in [n_f]$, where $n_f = 4$ denotes the index of feet. The compact form can be expressed as:

$$\boldsymbol{\phi}^\top = [\mathbf{r}^\top, \dot{\mathbf{r}}^\top, \ddot{\mathbf{r}}^\top, \boldsymbol{\theta}^\top, \dot{\boldsymbol{\theta}}^\top, \ddot{\boldsymbol{\theta}}^\top, \mathbf{p}_j^\top, \dot{\mathbf{p}}_j^\top, \ddot{\mathbf{p}}_j^\top, \mathbf{f}_j^\top]^\top \tag{2}$$

2) System Dynamics: We encode the system dynamics as a simplified single rigid body in Eq. (3), using a double integrator to replace the original Euler equation to keep the dynamics constraint convex. The whole system is discretized through Backward Euler integration with Δt between each time step.

$$\begin{bmatrix} \mathbf{r}[i+1] \\ \dot{\mathbf{r}}[i+1] \\ m\ddot{\mathbf{r}}[i] \\ \boldsymbol{\theta}[i+1] \\ \dot{\boldsymbol{\theta}}[i+1] \end{bmatrix} = \begin{bmatrix} \mathbf{r}[i] + \Delta t \cdot \dot{\mathbf{r}}[i+1] \\ \dot{\mathbf{r}}[i] + \Delta t \cdot \ddot{\mathbf{r}}[i+1] \\ \sum_j \mathbf{f}_j[i] + m\mathbf{g} \\ \boldsymbol{\theta}[i] + \Delta t \cdot \dot{\boldsymbol{\theta}}[i+1] \\ \dot{\boldsymbol{\theta}}[i] + \Delta t \cdot \ddot{\boldsymbol{\theta}}[i+1] \end{bmatrix} \tag{3}$$

where m is the robot mass and g is the gravity term.

3) Cost Function: The cost function consists of tracking costs and regularization terms governed by diagonal matrices $\mathbf{Q}$ and $\mathbf{R}$.

$$\mathbf{C} = \delta\boldsymbol{\phi}_Q[i]^T \mathbf{Q}\, \delta\boldsymbol{\phi}_Q[i] + \boldsymbol{\phi}_R[i]^T \mathbf{R} \boldsymbol{\phi}_R[i] \tag{4}$$

where $\delta\boldsymbol{\phi}_Q$ and $\boldsymbol{\phi}_R$ are defined as:

$$\delta\boldsymbol{\phi}_Q = \begin{bmatrix} \mathbf{r} - \mathbf{r}_{\text{ref}} \\ \boldsymbol{\theta} - \boldsymbol{\theta}_{\text{ref}} \\ \mathbf{p}_j - \mathbf{p}_j^{\text{ref}} \end{bmatrix}, \boldsymbol{\phi}_R = \begin{bmatrix} \ddot{\mathbf{r}} \\ \ddot{\boldsymbol{\theta}} \\ \ddot{\mathbf{p}}_j \\ \mathbf{f}_j \end{bmatrix} \tag{5}$$

Tracking costs include deviation from the desired base and foot EE trajectories. The regularization term includes minimizing the base acceleration, Euler angle acceleration, EE acceleration, and contact forces to encourage motion smoothness. The weights for the tracking terms are defined in Table I.

4) Safe Region Constraint: To incorporate safe region constraints for selecting proper footholds, we introduce binary variables $\mathbf{H}_{r,k,j}$, with r, k, and j expressing the r^{th} convex region, k^{th} footstep, and j^{th} foot and $r \in [R], k \in [n_s]$. One footstep is defined as a full swing phase for a foot. We use n_s and R to represent the number of footsteps specified by the gait configuration and the number of convex terrain polygons to be considered. For example, Fig. 4 shows a case with eight polygons. Eqs. (6) - (7) restrict the robot's EE to stay within one of the convex polygons when the corresponding binary variable $\mathbf{H}_{r,k,j}$ is True. Each polygon is parameterized by an inequality constraint ($\mathbf{A}_r$ and $\mathbf{b}_r$) that defines multiple half-spaces, along with an equality constraint ($\mathbf{A}_{\text{eq},r}$ and $\mathbf{b}_{\text{eq},r}$) that ensures the foothold position lies on a 3D plane. We use $\mathcal{C}_{k,j}$ to denote the set of time steps indicating stance after the k^{th} footstep for the j^{th} foot and the safe region constraint only applies to the first stance time step represented as $\mathcal{C}_{k,j}[0]$. Note that, during the offline phase, the terrain polygons are homogeneous and predefined.

$$\forall r \in [R], k \in [n_s], j \in [n_f]$$
$$\mathbf{H}_{r,k,j} \Rightarrow \mathbf{A}_r \mathbf{p}_j[i] \leq \mathbf{b}_r, \forall i \in \mathcal{C}_{k,j}[0] \tag{6}$$
$$\mathbf{A}_{\text{eq},r} \mathbf{p}_j[i] = \mathbf{b}_{\text{eq},r}, \forall i \in \mathcal{C}_{k,j}[0] \tag{7}$$
$$\sum_{r=0}^{R-1} \mathbf{H}_{r,k,j} = 1 \tag{8}$$
$$\mathbf{H}_{r,k,j} \in \{0, 1\} \tag{9}$$

5) Frictional and Contact Constraints: Frictional constraints are defined in Eqs. (10) - (11), with $\mathbf{n}_r$ and $\mathcal{F}_r$ as the normal vector and friction cone of the r^{th} convex region corresponding to the x and y dimensions of the EE position $\mathbf{p}_j^{xy}$. Contact constraints in Eqs. (12) - (13) forces the EE velocity to be zero during stance phase and the contact force to be zero during the non-contact phase. $\mathcal{C}_j$ represents the set of all time steps indicating stance for the j^{th} foot.

$$\forall r \in [R], k \in [n_s], j \in [n_f]$$
$$\mathbf{H}_{r,k,j} \quad \Rightarrow \quad \mathbf{f}_j[i] \cdot \mathbf{n}_r(\mathbf{p}_j^{xy}[i]) \geq 0, \ \forall i \in \mathcal{C}_{k,j} \tag{10}$$
$$\mathbf{f}_j[i] \in \mathcal{F}_r(\mu, \mathbf{n}_r, \mathbf{p}_j^{xy}[i]), \ \forall i \in \mathcal{C}_{k,j} \tag{11}$$
$$\dot{\mathbf{p}}_j[i] = 0, \ \forall i \in \mathcal{C}_j \tag{12}$$
$$\mathbf{f}_j[i] = 0, \ \forall i \notin \mathcal{C}_j \tag{13}$$

where μ denotes the friction coefficient.

6) Actuation Constraint: Since the joint angles are omitted in the single rigid body model, we use a fixed Jacobian $\mathbf{J}_j(\mathbf{q}_j^{\text{ref}})$ at a nominal joint pose $\mathbf{q}_j^{\text{ref}}$ for each leg to approximately consider the torque limit constraint in Eq. (14). In addition, since the translational and angular motions are decoupled, another actuation constraint on the angular acceleration is also added in Eq. (15).

$$\forall i \in [N], j \in [n_f]$$
$$\mathbf{J}_j(\mathbf{q}_j^{\text{ref}})^\top \mathbf{f}_j[i] \leq \boldsymbol{\tau}_{\max} \tag{14}$$
$$\mathbf{I}\ddot{\boldsymbol{\theta}}[i] \leq \boldsymbol{\tau}'_{\max} \tag{15}$$

where $\boldsymbol{\tau}_{\max}$ is the joint torque limit, $\boldsymbol{\tau}'_{\max}$ is the torque limit applied on the base, and $\mathbf{I}$ is the moment of inertia for the approximated single rigid body.

7) Kinematics Constraint: Lastly, the kinematics constraint in Eq. (16) strictly limits the possible EE movements to assure safety. Due to the convex nature of this MICP, we can determine the feasibility of a possible symbolic transition by checking if the optimal solution exists.

$$\mathbf{p}_j[i] \in \mathcal{R}_j({}^{\mathcal{B}}\mathbf{p}_j^{\text{ref}}, \mathbf{r}[i], \boldsymbol{\theta}_{\text{ref}}, \mathbf{p}_j^{\max}), \forall i \in [N], j \in [n_f] \quad (16)$$

where $\mathcal{R}_j$ is defined as a 3D box constraint around a nominal foot EE position based on the base position and orientation, and constrained by a maximum deviation $\mathbf{p}_j^{\max}$. Note that the reference orientation $\boldsymbol{\theta}_{\text{ref}}$ is used to avoid nonlinear constraint keep the problem convex.

B. Task Specification Encoding

After acquiring a set of feasible robot skills, we encode the skills into the specification φ as part of the environment safety assumptions $\varphi_{\text{e}}^{\text{t}}$ and system safety guarantees $\varphi_{\text{s}}^{\text{t}}$.

The skill assumptions $\varphi_{\text{e}}^{\text{t,skill}}$ encode the postconditions of the skills. The assumptions ensure that after the skill execution when the precondition holds, at least one postcondition of the skill must hold:

$$\varphi_{\text{e}}^{\text{t,skill}} \coloneqq \bigwedge_{o\in\mathcal{O}} \square((o \wedge \bigvee_{\sigma\in\Sigma_o^{\text{pre}}} \bigwedge_{\pi\in\mathcal{I}_{\text{robot}}\cup\mathcal{I}_{\text{terrain}}} \pi = \sigma(\pi)) \rightarrow \bigvee_{\sigma\in\Sigma_o^{\text{post}}} \bigwedge_{\pi\in\mathcal{I}_{\text{robot}}} \bigcirc(\pi = \sigma(\pi))) \quad (17)$$

In Example 1, the postcondition of skill o_0 is defined as

$$\square(o_0 \wedge \pi_{x_1} \wedge \pi_{y_1} \wedge n_{x_1}^{y_0} = 1 \wedge n_{x_1}^{y_1} = 1 \wedge n_{x_1}^{y_2} = 1 \wedge \ldots \rightarrow \bigcirc\pi_{x_0} \wedge \bigcirc\pi_{y_1} \wedge \neg\ldots) \quad (18)$$

The skill guarantees $\varphi_{\text{s}}^{\text{t,skill}}$ encodes the preconditions of the skills. The guarantees impose restrictions on when a skill can be executed. The guarantees only allow the robot to execute a skill if one of the skill's preconditions holds:

$$\varphi_{\text{s}}^{\text{t,skill}} \coloneqq \bigwedge_{o\in\mathcal{O}} \square(\neg(\bigvee_{\sigma\in\Sigma_o^{\text{pre}}} \bigwedge_{\pi\in\mathcal{I}_{\text{robot}}\cup\mathcal{I}_{\text{terrain}}} \bigcirc(\pi = \sigma(\pi))) \rightarrow \neg \bigcirc o) \quad (19)$$

In Example 1, the precondition of skill o_0 is defined as

$$\square\big(\neg(\bigcirc\pi_{x_1} \wedge \bigcirc\pi_{y_1} \wedge \bigcirc n_{x_1}^{y_0} = 1 \wedge \bigcirc n_{x_1}^{y_1} = 1 \wedge \bigcirc n_{x_1}^{y_2} = 1 \wedge \ldots) \rightarrow \neg \bigcirc o_0\big) \quad (20)$$

The hard constraints $\varphi_{\text{e}}^{\text{t,hard}}$ and $\varphi_{\text{s}}^{\text{t,hard}}$ are constraints that a repair cannot modify (see Sec. VI-C). Our system's hard constraints $\varphi_{\text{s}}^{\text{t,hard}}$ only allow the robot to execute one skill at a time: $\square\big(\neg(\bigcirc o \wedge \bigcirc o')\big)$, for any two different skills $o, o' \in \mathcal{O}$. Given that, we encode the following hard assumptions $\varphi_{\text{e}}^{\text{t,hard}}$:

(i) the uncontrollable terrain and request inputs cannot change during execution: $\square(\pi \leftrightarrow \bigcirc\pi)$, $\forall\pi \in \mathcal{I}_{\text{terrain}} \cup \mathcal{I}_{\text{req}}$, and

(ii) the robot inputs $\mathcal{I}_{\text{robot}}$ remain unchanged if no skill is executed: $\square\big(\bigwedge_{o\in\mathcal{O}} \neg o \rightarrow \bigwedge_{\pi\in\mathcal{I}_{\text{robot}}} (\pi \leftrightarrow \bigcirc\pi)\big)$.

C. High-level Manager and Symbolic Repair

We design a high-level manager to efficiently synthesize controllers for the encoded specification under given sets of terrain and request states. The manager takes in the specification φ, a predefined set of terrain states $\Sigma_{\text{terrain}}^{\text{poss}} \subseteq \Sigma_{\text{terrain}}$, and a predefined set of request states $\Sigma_{\text{req}}^{\text{poss}} \subseteq \Sigma_{\text{req}}$. For every pair of integer terrain and request state $(\sigma_{\text{terrain}}, \sigma_{\text{req}}) \in \Sigma_{\text{terrain}}^{\text{poss}} \times \Sigma_{\text{req}}^{\text{poss}}$, the manager first translates the integer terrain state $\sigma_{\text{terrain}} : \mathcal{I}_{\text{terrain}} \rightarrow [n_t]$ to its corresponding Boolean terrain state $\sigma_{\text{terrain}}^{\mathcal{B}} : \mathcal{I}_{\text{terrain}}^{\mathcal{B}} \rightarrow \{\texttt{True}, \texttt{False}\}$, using a set of Boolean propositions $\mathcal{I}_{\text{terrain}}^{\mathcal{B}}$ to represent the integer terrain inputs $\mathcal{I}_{\text{terrain}}$, as done in [87]. We overload $\sigma_{\text{terrain}}^{\mathcal{B}}$ and σ_{req} to represent the inputs that are `True` in $\sigma_{\text{terrain}}^{\mathcal{B}}$ and σ_{req}. The manager then generates a partial evaluation $\varphi' \coloneqq \varphi[\sigma_{\text{terrain}}^{\mathcal{B}} \cup \sigma_{\text{req}}, \mathcal{I}_{\text{terrain}}^{\mathcal{B}} \cup \mathcal{I}_{\text{req}} \setminus \sigma_{\text{terrain}}^{\mathcal{B}} \cup \sigma_{\text{req}}]$ (see Definition 1). Next, we remove skills that cannot be executed in the local environment, i.e., their preconditions are evaluated to `False` under the partial evaluation. Since the inputs of φ' only include the robot inputs $\mathcal{I}_{\text{robot}}$ and the outputs of φ' consist of fewer skills, we avoid the exponential blow-up of the synthesis algorithm in the size of the variables. Lastly, the manager synthesizes a strategy $\mathcal{A}_{\varphi'}$ for each φ'.

The partial evaluation φ' can be unrealizable if the gait-fixed MICP-based physical feasibility checking in Sec. VI-A does not generate enough skills for the robot to reach the requested goal under the terrain state. To add more robot skills, we will leverage a gait-free MICP (formulated in Sec. VI-D) which retains all continuous decision variables and constraints from the gait-fixed MICP but modifies the contact state-dependent constraints so that the contact sequence and timing are no longer fixed. Since such a gait-free MICP is computationally expensive, we leverage a symbolic repair tool [28] to generate symbolic suggestions that guide us to perform necessary gait-free MICP only. Given an unrealizable φ', symbolic repair systematically modifies the pre- and postconditions of existing skills to suggest new skills that make φ' realizable, if such skills exist and are physically feasible. Fig. 2(c) illustrates the use of repair in Example 1. To create a skill that reaches the requested grid (x_0, y_0), repair selects the skill transition that moves the robot from the grid (x_1, y_0) to (x_2, y_0), and modifies the postcondition to be (x_0, y_0).

D. Gait-Free MICP

We aim to implement the suggested skills by reconfiguring the contact sequence and timing to generate new locomotion gaits. This can be achieved by solving a gait-free version of MICP in Eq. (1). The gait-free MICP retains all continuous decision variables and constraints from the gait-fixed MICP but modifies the contact state-dependent constraints, as the contact sequence and timing are no longer fixed. Instead of using $\mathbf{H}_{r,k,j}$, we introduce a different set of binary variables $\mathbf{H}_{r,m,j}$ for defining the contact state for each foot at each time step explicitly. r and j still represent the r^{th} convex region and j^{th} foot, respectively, while $m \in [M]$ denotes the m^{th} time step, evenly discretized with Δt_m over the entire M time steps. We use $\mathcal{O}_{m,m+1}$ to denote the set of continuous time

steps that span from the m^{th} to the $m+1^{\text{th}}$ binary time step. As a result, the following constraints are modified:

1) Safe Region Constraint: The safe region constraint is defined in Eq. (21) - (22) similar to the gait-fixed case in Eq. (6) - (7) when a binary variable $\mathbf{H}_{r,m,j}$ is activated. Different from Eq (8), the summation of the binary variables at m^{th} time step for the j^{th} foot is allowed to be zero to generate a swing phase as shown in Eq. (23).

$$\forall r \in [R], m \in [M], j \in [n_f]$$

$$\mathbf{H}_{r,m,j} \Rightarrow \mathbf{A}_r \mathbf{p}_j[i] \leq \mathbf{b}_r, \forall i \in \mathcal{O}_{m,m+1} \tag{21}$$

$$\mathbf{A}_{\text{eq},r} \mathbf{p}_j[i] = \mathbf{b}_{\text{eq},r}, \forall i \in \mathcal{O}_{m,m+1} \tag{22}$$

$$\sum_{r=0}^{R-1} \mathbf{H}_{r,m,j} \leq 1 \tag{23}$$

$$\mathbf{H}_{r,m,j} \in \{0,1\} \tag{24}$$

2) Frictional and Contact Constraints: Different from the gait-fixed case in Eq. (10) - (13), the activation of frictional and contact constraints is purely decided by the binary variables.

$$\forall r \in [R], m \in [M], j \in [n_f]$$

$$\mathbf{H}_{r,m,j} \;\Rightarrow\; \mathbf{f}_j[i] \cdot \mathbf{n}_r(\mathbf{p}_j^{xy}[i]) \geq 0, \forall i \in \mathcal{O}_{m,m+1} \tag{25}$$

$$\mathbf{f}_j[i] \in \mathcal{F}_r(\mu, \mathbf{n}_r, \mathbf{p}_j^{xy}[i]), \forall i \in \mathcal{O}_{m,m+1} \tag{26}$$

$$\sum_{r=0}^{R-1} \mathbf{H}_{r,m,j} = 1 \;\Rightarrow\; \dot{\mathbf{p}}_j[i] = 0, \forall i \in \mathcal{O}_{m,m+1} \tag{27}$$

$$\sum_{r=0}^{R-1} \mathbf{H}_{r,m,j} = 0 \;\Rightarrow\; \mathbf{f}_j[i] = 0, \forall i \in \mathcal{O}_{m,m+1} \tag{28}$$

Compared to gait-fixed MICP, gait-free MICP introduces more binary variables to determine contact states, resulting in longer computation times. As such, it is only triggered after performing symbolic repair.

VII. Online Execution

Due to the inevitable disparity between offline synthesis and real-world online terrain conditions, such as variations in terrain shape and position, additional efforts are required to bridge this gap and prevent potential execution failures. The online execution module takes in terrain states $\sigma_{\text{terrain}} \subseteq \mathcal{I}_{\text{terrain}}$ after abstracting the terrain polygons online, a request state $\sigma_{\text{req}} \subseteq \mathcal{I}_{\text{req}}$, and a strategy $\mathcal{A}$ from the offline synthesis module (Sec. VI). This module then executes the strategy automaton $\mathcal{A}$ by solving a MICP problem online again with the actual perceived terrain polygons, potentially different from the ones abstracted offline, to generate a reference trajectory for each transition (Sect. VII-A). This reference trajectory along with the corresponding contact information will be further tracked by a tracking controller in real time (Sec. VIII). As shown by the blue lines in Fig. 3(c), if the robot encounters an unseen terrain state, we leverage online symbolic repair to create new skills that handle the unexpected terrain state and failure transition at runtime (Sec. VII-B). After reaching the request state σ_{req}, the robot resets the strategy with a new terrain state, request goal states, and repeats the execution until reaching the final goal state.

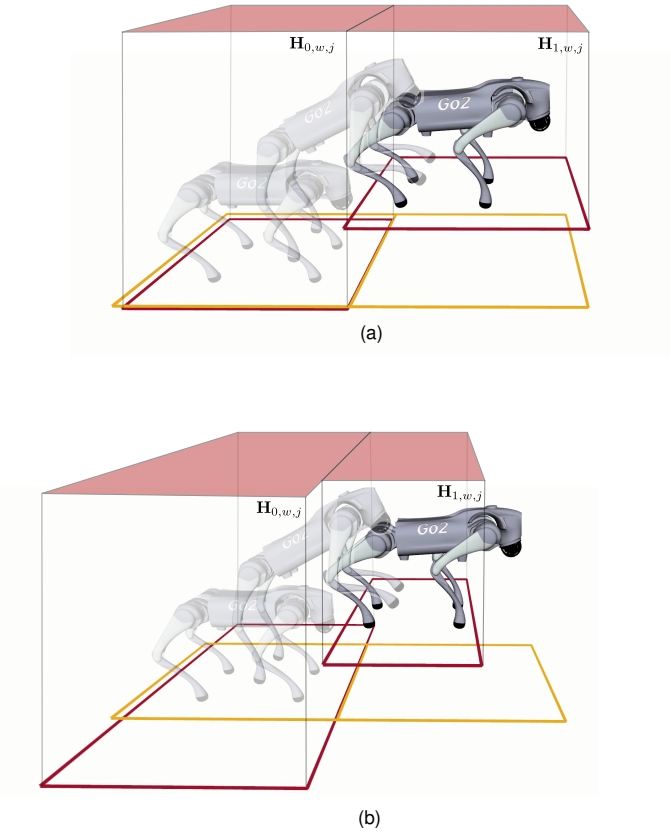

Fig. 5. Demonstrations of (a) offline MICP for a skill transitioning from a flat terrain to a high terrain with predefined polygons; (b) online MICP for the same skill but with online terrain polygons.

A. Strategy Automaton Execution and Online MICP Modifications

The red path in Fig. 3(c) represents the automaton online execution process. Before transitioning to the new symbolic state, an online gait-fixed MICP is solved according to the skill provided by the automaton. The automaton advances only if the MICP successfully finds a solution. Slightly different from the gait-fixed MICP formulation during the offline phase, the online gait-fixed MICP is executed given accurate terrain information from a terrain segmentation module. For example, a skill transitioning from flat terrain to high terrain, as shown in Fig. 5(a), uses predefined, homogeneous terrain polygons for feasibility check during offline synthesis. Given that, Fig. 5(b) illustrates how the terrain polygons detected online for the same skill may differ from the offline ones in both position and geometry. In addition, the following modifications are highlighted when attempting to transition between two symbolic states in the automaton.

1) Robot Pose Re-Targeting: Since the final targeting condition significantly influences the reference trajectory and the feasibility of the MICP problem, we evaluate the final condition by solving a kinematic feasibility problem (a simplified MICP in Eq. (1)) before solving the online MICP. Compared with the gait-fixed MICP, the dynamics equation (3) is replaced by enforcing the center of mass (CoM) to lie inside a convex

support polygon with all feet in stance to ensure static stability. In addition, a hard constraint is added to ensure that the modified robot pose stays within a certain threshold compared with the original desired pose. The cost function is simplified to stay as close as possible to the original desired pose. The higher-order terms of body position, orientation, and end-effectors are excluded from the decision variables. All the other constraints not involving those higher-order terms remain the same. Once the kinematic feasibility problem is solved successfully, the online MICP is solved using the modified re-targeted final condition and reference trajectory.

2) Collision Avoidance and Swing Foot Constraints: Since the trajectory generated by the online gait-fixed MICP is directly sent to a tracking control module later, high-quality end-effector (EE) trajectories are crucial to ensure collision avoidance and sufficient swing foot clearance from the terrain. To achieve this, we first introduce more binary variables $\mathbf{H}_{s,w,j}$ for defining the collision-free region selection for the j^{th} foot at each time step. Specifically, $s \in [S]$ represents the s^{th} convex collison-free region and $w \in [W]$ denotes the w^{th} time step, evenly discretized with Δt_w over the entire W time steps. Fig. 5(b) demonstrates two collision-free regions.

$$\forall s \in [S], w \in [W], j \in [n_f]$$
$$\mathbf{H}_{s,w,j} \Rightarrow \mathbf{A}_s \mathbf{p}_j[i] \leq \mathbf{b}_s, \forall i \in \mathcal{C}_{w,w+1} \tag{29}$$
$$\sum_{s=0}^{S-1} \mathbf{H}_{s,w,j} = 1 \tag{30}$$
$$\mathbf{H}_{s,w,j} \in \{0,1\} \tag{31}$$

where $\mathcal{C}_{w,w+1}$ denotes the set of continuous time steps that span from the w^{th} to the $w+1^{\text{th}}$ binary time step.

To enable larger swing foot clearance from the terrain in case of non-trivial tracking errors, we also add constraints to force the swing foot height above a user-defined threshold h_{swing}, given the fixed contact timing.

Note that the collision avoidance and swing foot constraints are also incorporated during the offline MICP as part of the feasibility checking rules. However, we highlight it here due to its critical impact on the tracking performance.

B. Runtime Repair

The runtime repair takes in a terrain state $\sigma_{\text{terrain}} \in \Sigma_{\text{terrain}}$, a request state $\sigma_{\text{req}} \in \Sigma_{\text{req}}$, and a Boolean formula $\varphi_{\text{disallow}}$ representing disallowed transitions discovered at runtime. We first update the system hard constraint $\varphi_{\text{s}}^{\text{t}}$ in the specification φ from Sec. VI-B to be $\varphi_{\text{s}}^{\text{t}} \wedge \square\varphi_{\text{disallow}}$, so that the updated specification respects the newly discovered disallowed transitions, if any. We then leverage the high-level manager to create a partial evaluation of φ over σ_{terrain} and σ_{req}, and perform symbolic repair to generate new robot skills and a new strategy to handle σ_{terrain} and σ_{req}, as done in Sec. VI-C.

VIII. Tracking Control

The tracking control module adopts an MPC-Whole-Body-Control (WBC) hierarchy, ensuring precise end-effector (EE) and centroidal momentum tracking. To smoothly and efficiently execute the strategy considering the potential computational delay in solving MICP, a harmonic coordination module between the strategy automaton roll-out and the tracking module is designed (Sec. VIII-B).

A. Tracking Control Module

1) Nonlinear Model Predictive Control (NMPC): The NMPC operates independently from the symbolic planning module, tracking reference trajectories generated by the online MICP using a more accurate dynamics model. In this work, the NMPC accounts for the robot's centroidal dynamics and kinematics, similar to approaches in [89]–[91], presenting a more accurate model than the simplified angular dynamics in the MICP. An analytical inverse kinematics solution based on the MICP output provides the full joint state reference trajectory for the NMPC. In addition to standard frictional and contact constraints and base tracking costs, an additional cost function for EE reference tracking from the MICP is included to enhance precision. The NMPC optimization problem is formulated as a Sequential Quadratic Program (SQP) and solved using the OCS2 library [92], with a time horizon of one second and 100 knot points.

2) Whole-Body Control (WBC): While NMPC operates at the centroidal level to generate dynamically feasible trajectories, WBC ensures precise execution by resolving full-body state control, including joint torques, accelerations, and contact forces. The whole-body controller tracks the NMPC trajectory by solving a weighted quadratic program (QP) [93] at 500 Hz. To improve the performance of agile motions such as leaping and jumping, centroidal momentum tracking [94] is included. This MPC-WBC hierarchy allows the system to handle both centroidal-dynamics-level and full-body-dynamics-level control in a coordinated manner, ensuring robustness in real-world deployment especially for highly dynamic motions such as jumping.

3) State Estimation: The state estimator employs a linear Kalman filter similar to that in [95], with the addition of OptiTrack motion capture (mocap) measurements fused alongside IMU data and joint encoder readings to achieve accurate body position estimation. For agile motions such as jumping, we observed improved base-height estimation by assigning higher noise values to the mocap feedback during aerial phases, due to its limited 120 Hz update rate.

B. Coordination between Strategy Execution and Tracking Module

Due to the potential delays in solving MICP during the strategy automaton roll-out, a harmonic coordination between the strategy execution and tracking control module is essential. The tracking module's reference trajectory is updated dynamically alongside the strategy execution process, as shown in Fig. 6. The overall process can be summarized as follows:

1) Strategy Execution: The strategy automaton execution thread begins by solving the online gait-fixed MICP, starting from State 0 in the automaton. Once the MICP solution

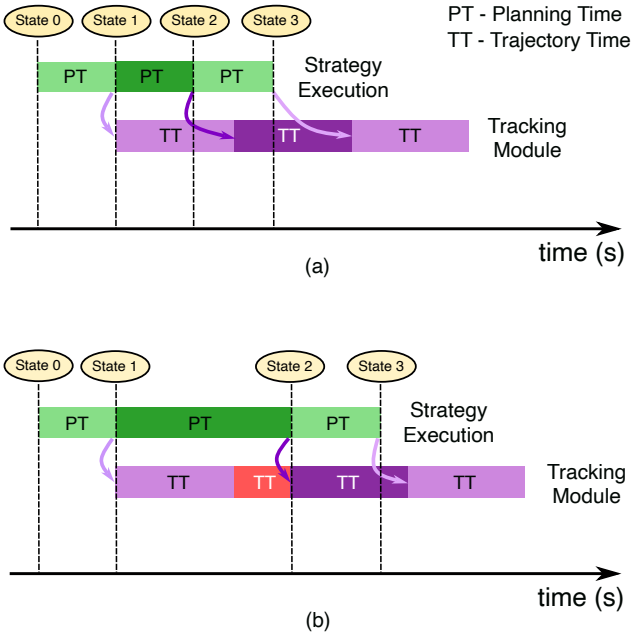

Fig. 6. Coordination between strategy execution and tracking control module. (a) The MICP solving time (denoted by PT) for transitioning from State 1 to State 2 is shorter than the time horizon of the previous reference trajectory (denoted by TT), allowing the seamless appending for the new trajectory. (b) The MICP solving time exceeds the time horizon of the previous reference trajectory, requiring the robot to come to a stop (red) and wait for the new trajectory whenever available.

is obtained, it immediately sends the reference trajectories and corresponding contact information to the tracking control module. The automaton then progresses to the next transition, using the final condition in the previous trajectory segment as the new initial condition. In Fig. 6, the colored blocks in the strategy execution timeline indicate the time taken for each MICP solve during the automaton roll-out. PT and TT denote the planning time and trajectory time, respectively.

2) Tracking Control Module: The MPC-WBC tracking control module receives time-indexed reference trajectories, which can be updated in real-time. After completing the tracking of the current reference trajectory, the robot returns to a stance phase, ready to accept new reference trajectories. As depicted in Fig. 6, the colored blocks in the tracking control module represent the time horizon of each reference trajectory sent by the strategy execution thread. Once the initial reference trajectory is generated, the MPC-WBC thread begins tracking it using more accurate dynamics models, as described in Sec.VIII.

3) Delay Handling: For more complex scenarios involving a larger number of terrain polygons, the MICP solving time may increase and exceed the time horizon of the generated reference trajectory. Fig. 6(a) and (b) illustrate two cases of MICP solving times: Case (a): The solving time for transitioning from automaton State 1 to State 2 is shorter than the time horizon of the previous reference trajectory. In this case, the new reference trajectory is seamlessly appended to the existing one, and the robot continues tracking the previous trajectory.

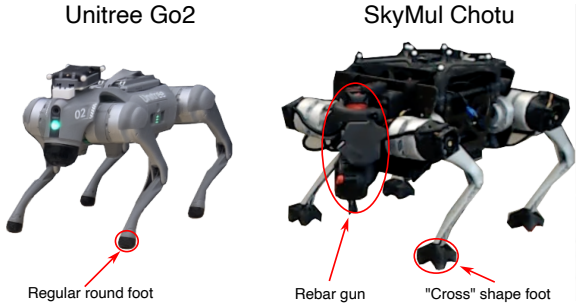

Fig. 7. Hardware platforms used for experiments: Unitree Go2 and SkyMul Chotu (equipped with a rebar gun and "cross"-shaped feet).

TABLE II
ROBOT PARAMETERS

Parameter	Unitree Go2	SkyMul Chotu
m (kg)	15	20
$\boldsymbol{\tau}_{\max}$ (N · m)	(23.5, 23.5, 45.4)	(23.5, 23.5, 33.5)
$\mathbf{q}_j^{\text{ref}}$ (rad)	(0.0, 0.72, -1.44)	(0.0, 0.72, -1.44)
${}^{\mathcal{B}}\mathbf{p}_j^{\text{ref}}$ (m)	(0.1805, 0.1308, -0.29)	(0.2118, 0.210, -0.30)
$\mathbf{p}_j^{\max}$ (m)	(0.15, 0.1, 0.15)	(0.15, 0.1, 0.15)
$\mathbf{I}$ (kg · m^2)	diag(0.152, 0.369, 0.388)	diag(0.396, 0.915, 1.107)

Case (b): The solving time exceeds the time horizon of the previous reference trajectory, and the robot has already entered a stance phase (red block) when the MICP solution is obtained. In this case, the robot waits until the newly generated reference trajectory is sent based on the current system time (red block in Fig. 6 (b)).

IX. SIMULATION

We present examples of maneuvering across diverse environments in a Gazebo simulation to demonstrate the framework's efficacy, scalability, and generalizability. Case studies on online execution highlight our framework's capability to handle unforeseen terrains and failures. Benchmarking experiments are also conducted to further compare our proposed framework with pure MIP approaches.

A. Robot Setup

As shown in Fig. 7, we verify our algorithms on two separate robot platforms, Unitree Go2 and SkyMul Chotu (a modified Unitree Go1 robot dedicated for rebar tying tasks). The SkyMul Chotu is equipped with a rebar gun mounted on its head and customized "cross"-shaped feet designed for reliable standing on rebars. Note that in simulation, this foot shape is simplified to a regular round foot to avoid the complexity of simulating contact with irregular surfaces. In our planner, we model both cases as point contact. The parameters for each robot are defined in Table II and used in our implementation, including the robot mass m, torque limit $\boldsymbol{\tau}_{\max}$ and the reference joint position $\mathbf{q}_j^{\text{ref}}$ for a single leg with three joints, the reference foot position relative to the base frame ${}^{\mathcal{B}}\mathbf{p}_j^{\text{ref}}$ and the maximum deviation of the foot position $\mathbf{p}_j^{\max}$ for the front left leg ($j = 0$), and the moment of inertia of the approximated single rigid body $\mathbf{I}$.

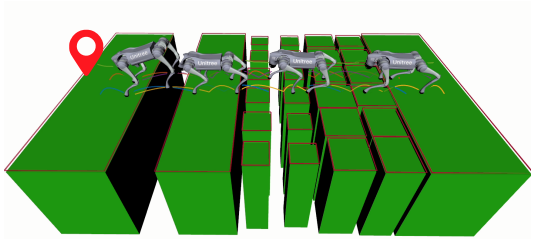

(a) Unstructured - 4

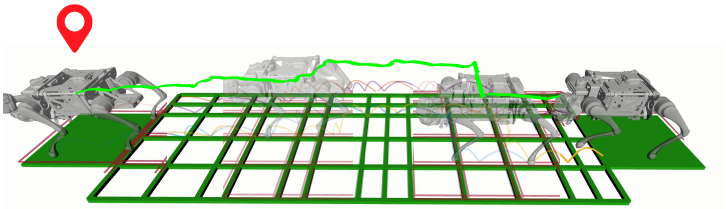

(c) Rebar - 7

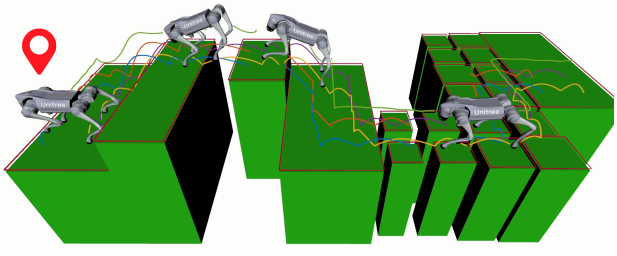

(b) Unstructured - 8

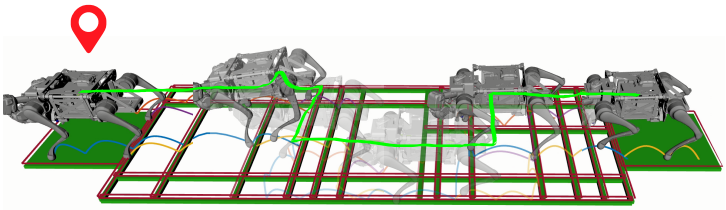

(d) Rebar - 14

Fig. 8. Unstructured and rebar terrain scenarios.

TABLE III
OFFLINE SYNTHESIS AND REPAIR TIME

Scenario	Grid Size	Terrain and Request State Pairs (Success/Total)	Number of Skills (Original/New/Total)	Symbolic Repair Time (s)	Feasibility Check Time (s) (Gait-Fixed/Gait-Free)
Unstructured - 4	3×3	169/169	18/13/64	8.07	18.97/449.94
	5×5	129/158	19/9/64	77.16	20.26/241.42
Unstructured - 8	3×3	250/264	19/20/256	14.90	22.92/382.63
	5×5	179/246	20/16/256	93.21	18.59/196.88
Rebar - 7	3×3	196/196	18/11/196	7.44	15.63/417.55
	5×5	196/196	18/10/196	21.63	14.83/374.89
Rebar - 14	3×3	237/237	20/29/784	10.34	21.92/701.38
	5×5	196/196	20/18/784	24.31	23.06/453.94

B. Simulation Environment Setup

To demonstrate the generalizability of the proposed framework, we evaluate it on two scenarios with varying terrain types, safe stepping regions, and robot platforms–Unitree Go2 and SkyMul Chotu. We model obstacles as a distinct terrain type, with obstacle avoidance encoded as hard constraints in φ_s^t, and the requested waypoint are assumed not to be obstacles. We test both 3×3 and 5×5 grid abstractions. The 5×5 grid has a longer planning horizon and greater decision complexity. We use a 0.8 m cell size for the unstructured terrain and 0.6 m for the rebar, which can be adjusted for practical applications.

1) Unstructured Terrain: We abstract 8 terrain types–*flat terrain*, *high terrain*, *low terrain*, *dense stone*, *sparse stone*, *gap*, *high gap*, and *low gap*–with classification criteria based on polygon heights, counts, and areas relative to the abstracted cells. Note that a terrain is classified as a *gap* when the ratio of its overlapping area with the abstracted cell falls below a threshold. We define two terrain configurations, one with four selected terrain types and another with all eight terrain types, as shown in Figs. 8(a) and 8(b).

2) Rebar Terrain: Inspired by automating labor-intensive rebar tying tasks on construction sites [73], we explore a second case study where the quadrupedal robot navigates a rebar mat. We model each rebar as a rectangular polygon with a 3 cm width. Unlike the stepping stone scenario, this setup offers a larger number of potential stepping polygons due to the higher rebar density. Observing that the robot's traversability depends on rebar sparsity in different directions—whether aligned with the robot's facing direction or not, within a given tolerance—we abstract and classify rebar types based on a combination of horizontal sparsity (perpendicular to the robot's facing direction) and vertical sparsity (parallel to it). By calculating the number and relative spacing of the rebars inside each abstracted cell, we categorize each direction's sparsity as *dense* (0.05 - 0.15 m), *sparse* (0.15 - 0.35 m), or *extreme sparse* (above 0.35 m), *single*, *none*. To reduce the complexity of the problem, we remove some challenging combinations such as *none* or *single* in both directions and treat them as *obstacle*. As a result, we define two example configurations with 7 and 14 rebar terrain types. The 7-type scenario in Fig. 8(c) generates random rebar sparsity between 0.15 and 0.35 m, excluding the *extreme sparse* type. In contrast, the 14-type scenario in Fig. 8(d) includes rebar sparsity from 0.15 to 0.6 m, potentially covering more challenging combinations including the *extreme sparse* ones.

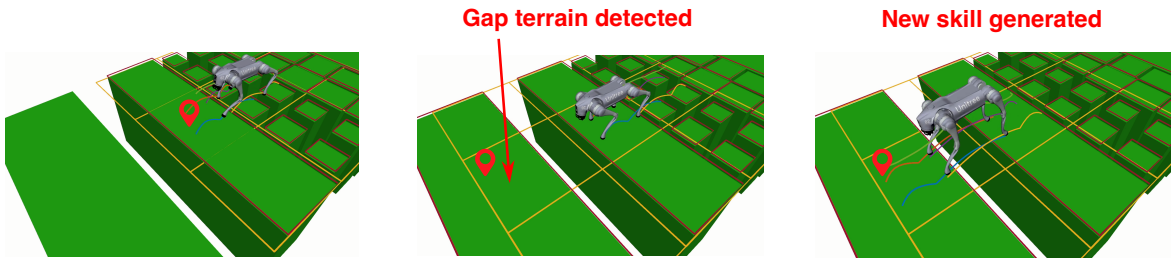

(a) Before a gap (b) Encountering a gap (c) After online repair

Fig. 9. Runtime repair scenario when encountering a gap.

TABLE IV
ONLINE GAIT-FIXED MICP SOLVING TIME FOR SIMULATION

Scenario	Collision Avoidance	Binary Variables	Continuous Variables	Number of Polygons	Solve Time (s)
Unstructured - 4	No	52	6583.5	6.5	0.37
Unstructured - 8	Yes	256	5166	2	2.65
	No	69	7938	7.5	0.49
Rebar - 7	No	70	7938	7.875	1.11
Rebar - 14	No	58	8142.75	6.25	1.09

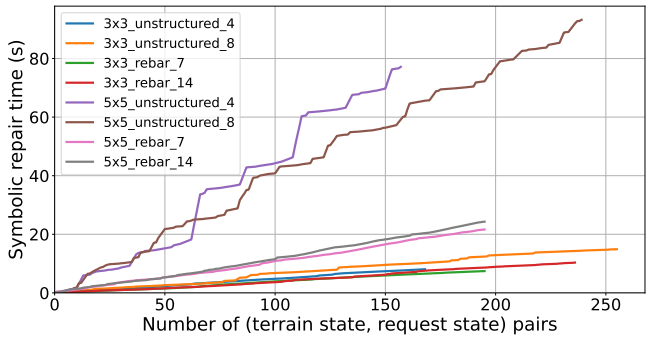

Fig. 10. Symbolic repair time in the size of terrain and request state pairs.

C. Offline Synthesis Results

We evaluate the offline synthesis module for both *Unstructured* and *Rebar Terrain* by initializing the skills with two trotting gaits (2 s and 3 s). Before synthesis, we generate the set of possible terrain states $\Sigma^{\text{poss}}_{\text{terrain}}$ (supposedly provided by the user) by systematically sweeping a local grid across the entire terrain map based on the best available knowledge. The request states $\Sigma^{\text{poss}}_{\text{req}}$ are defined as the top row of the local grid map in the robot's facing direction, along with the two corner cells to allow additional movement directions.

Table III reports (i) the number of terrain and request states pairs $(\sigma_{\text{terrain}}, \sigma_{\text{req}}) \in \Sigma^{\text{poss}}_{\text{terrain}} \times \Sigma^{\text{poss}}_{\text{req}}$, including both successful and total ones, (ii) the number of skills, including the original, the newly discovered, and the total possible ones, and (iii) offline repair and feasibility checking times, including both from gait-fixed and gait-free MICP. We first note that repair solves 93.4% of the terrain and request state pairs. The rest are unrepairable because the request states are unreachable due to obstacles or physical infeasibility. As highlighted in red, the number of newly discovered skills is $71.6 - 97.6\%$ smaller than checking all possible skills, each of which corresponds to solving an expensive gait-free MICP that takes 27.23 s on average (max 145.66 s) for a new locomotion gait. This demonstrates that offline repair effectively minimizes the number of gait-free MICP solves.

To investigate the scalability of offline repair, we perform repair across various sizes of the terrain and request states. As shown in Fig. 10, the repair runtime grows linearly in the size of the terrain and request states for both 3×3 and 5×5 grids. While fewer terrain and request states handled offline reduce checked time, they may lead to more frequent unforeseen states during online execution. Moreover, we note that the slope of 5×5 cases in Fig. 10 are steeper than those of 3×3 as a result of the increased state space. On average, repair takes 478.1% more time for 5×5 grids than 3×3 for one terrain and request states pair. In practice, the perception range and the robot size limit the grid size, so we do not test beyond 5×5 grids, though the user can adjust the resolution.

D. Online Execution Results

Fig. 8 visualizes the snapshots of Go2 and Chotu traversing the terrains during online execution. The robot is tasked with reaching a global waypoint using a naive global shortest path planner. Specifically, the local waypoint in the local grid map is selected by choosing the closest, non-obstacle grid cell toward the global waypoint. Fig. 8(a) shows a maneuver traversing through flat terrain, dense stepping stone, sparse stepping stone, and a gap. Fig. 8(b) shows the robot navigate through all eight terrain types, including elevation variations by adaptively choosing the locomotion gaits. Similarly, Fig. 8(c) and (d) present rebar traversing in separate scenarios with potentially 7 and 14 rebar terrain types. Notably, the robot leverages a set of newly discovered leaping gaits with short aerial phases for transitions from lower to higher terrain or across gaps and extreme sparse rebars as shown in Fig. 8(b) and (d). Table IV presents the average number of decision variables

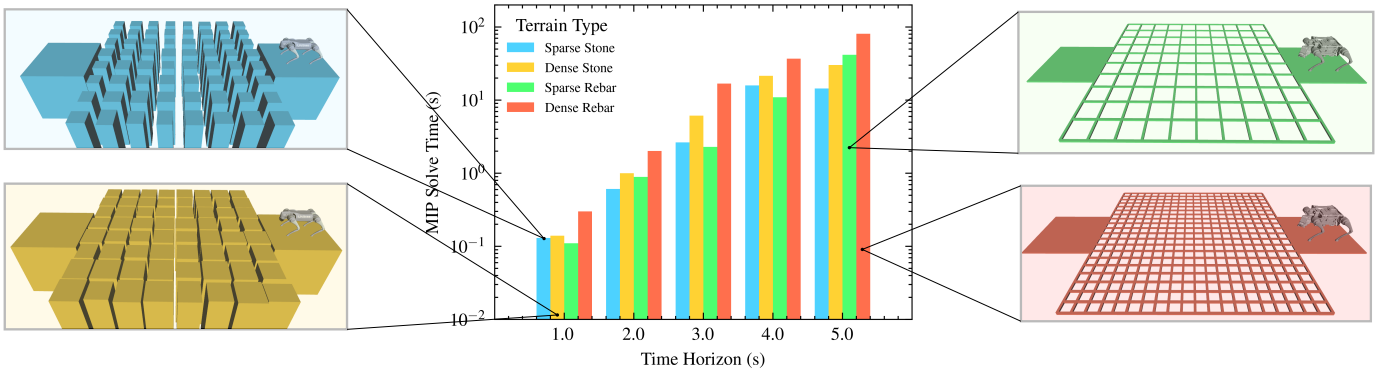

Fig. 11. MIP solve time benchmark. Four scenarios including sparse stepping stone (blue), dense stepping stone (yellow), sparse rebar (green), and dense rebar (red) are evaluated with time horizons ranging from 1 - 5 seconds. **Ye: [improve the lines of this figure as we discussed.]**

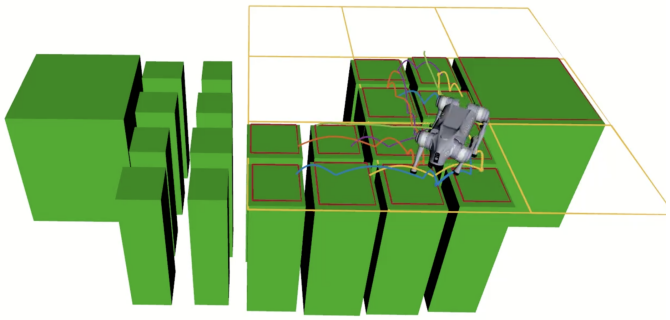

Fig. 12. Demonstration of the robot executing multiple turning behaviors to continuously progress toward the global waypoint on terrain arranged in a zig-zag pattern.

Ye: [why the number of continuous variables has decimal digits?]Ziyi: [The planner could choose adaptive gaits with different time horizons.] terrain polygons, and online gait-fixed MICP at runtime. On average, the online gait-fixed MICP takes 430 ms to solve the unstructured terrain cases and 1.1 s for rebar cases when the collision avoidance is disabled. The rebar scenarios exhibit 155.8% longer solve times due to their overlapping, skewed rebar arrangement, and a larger number of terrain polygons. Additionally, enabling collision avoidance (necessary for *Unstructured - 8* case to handle the elevation change) increases the number of binary variables by 271.0%, increasing the solve time by 440.8% (highlighted in red).

As a case study to demonstrate the capability of handling unforeseen terrains and failures during execution, we highlight the following run-time scenarios:

1) Unforeseen Terrain States: With limited knowledge of the global terrain polygons, the terrain states provided during offline synthesis may be insufficient when encountering new terrain configurations. Fig. 9 illustrates this in an Unstructured - 4 types scenario with a 3×3 grid size, where terrain states involving *gap* terrain are excluded, treating *gap* as an unseen terrain type during offline synthesis. When the robot reaches a new terrain state that includes a *gap*, we trigger runtime repair for the current terrain and request states. A new skill with a leaping gait is generated to successfully cross the gap. The runtime repair takes 12.36 s, where symbolic repair takes 0.18 s, and the gait-free MICP takes 12.18 s to generate the new leaping gait.

2) Solving Failure: Another common runtime failure arises from MICP solving failures. Due to discrepancies between the predefined polygons used in offline synthesis and the actual online terrains—such as variations in shape and size—a skill deemed feasible offline may become infeasible when executed online, even if classified under the same symbolic transition. Originally moving straight ahead, the detours shown as green lines in Fig. 8(c) and (d) illustrate the re-synthesis process triggered by solving failures in both the 7-type and 14-type cases. Solving failure occurs more frequently in the rebar scenario than in the unstructured terrain scenario due to uncertainties in the shapes and sizes of online rebar polygons. The runtime resynthesis takes 0.11 s and 0.07 s for the two cases respectively. Both cases do not trigger runtime repair because other existing skills suffice to navigate the robot to the goals under the solving failures.

E. Benchmark: Pure MIP Planner

To evaluate how the symbolic planning benefits the overall planning framework, we benchmark our method against pure MIP approaches, where we implement a planner to evaluate how computation time scales with the planning horizon and terrain complexity. Specifically, we examine five planning horizons ranging from 1 s to 5 s. In addition, we vary the terrain types by considering sparse stepping stones (0.15 m spacing), dense stepping stones (0.05 m spacing), sparse rebar (0.3 m spacing), and dense rebar (0.15 m spacing), as illustrated in Fig. 11 with specific colors.

The benchmarked planner is configured to solve only gait-fixed MICP; we omit gait-free MICP due to its significantly longer solve time in longer horizon setup that are more than 2 s. For a given planning horizon, the local planning region is linearly expanded to increase the traversable distance. The locomotion gait is repeated cyclically on a 1 s trotting pattern. During execution, the planner—similar to our proposed

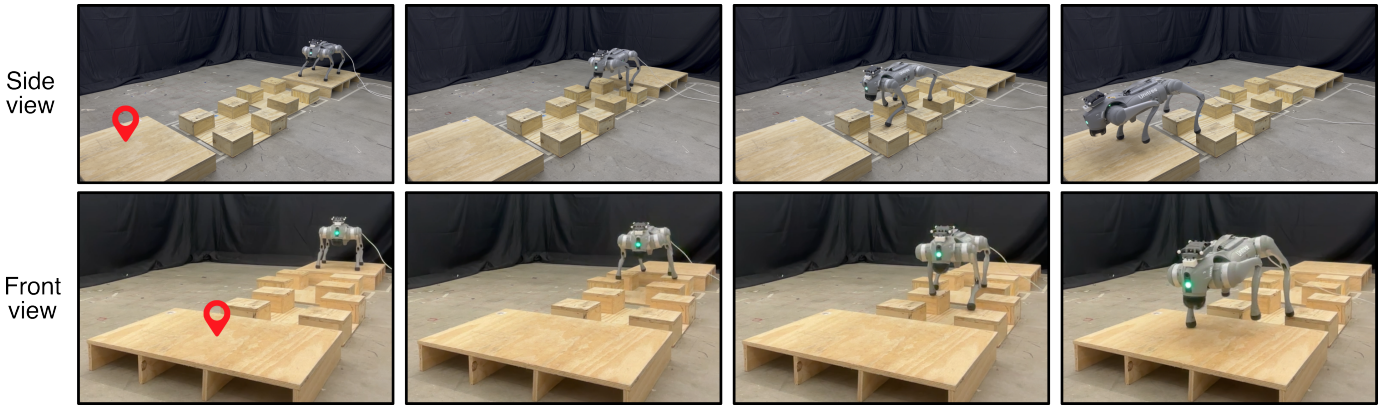

Fig. 13. Hardware experiment demonstration for the first unstructured terrain scenario with sparse stepping stones and flat terrains.

framework—receives a global waypoint and incrementally computes local waypoints, selecting the farthest reachable position within the local planning region.

As shown in Fig. 11, the histogram illustrates the average time to solve the MIP in different scenarios and time horizons. The results show that, within the same scenario, the MICP solve time increases almost exponentially with the planning horizon. Furthermore, dense rebar and stepping stone scenarios consistently require longer solve times than their sparse counterparts, due to the larger number of terrain segments involved in the optimization. In our proposed method, we primarily use 2 to 3 s gait horizons for each symbolic transition, striking a balance between computational efficiency and sufficient planning foresight. This choice avoids overly short myopic horizons, while still allowing for adaptive gait behaviors.

F. Extension: Locomotion with Yaw Command

In the previous examples, we assume that the yaw angle of the robot base is fixed to simplify the problem. However, the robot's physical capability to traverse terrains largely depends on the base orientation. For instance, performing a forward jump onto a high terrain is different from a sideway jump, in terms of both leg kinematics and dynamics. Therefore, to showcase the flexibility and generalizability of our framework, we provide an extension to the existing abstraction of the robot state to allow the orientation variation.

Specifically, the robot inputs are now defined as $\mathcal{I}_{\text{robot}} := \{\pi_x \mid x \in \mathcal{X}\} \cup \{\pi_y \mid y \in \mathcal{Y}\} \cup \{\pi_{yaw} \mid yaw \in \mathcal{W}\}$, where we define a new set of yaw angles $\mathcal{W} := \{-180°, -90°, 0°, 90°, 180°\}$. Note that, a finer discretization of the yaw angles can be defined as needed. Similarly, the request inputs are defined as $\mathcal{I}_{\text{req}} := \{\pi_x^{\text{req}} \mid x \in \mathcal{X}\} \cup \{\pi_y^{\text{req}} \mid y \in \mathcal{Y}\} \cup \{\pi_{yaw}^{\text{req}} \mid yaw \in \mathcal{W}\}$. The robot and the request input can be further divided into translational $\mathcal{I}_{\text{robot}}^{\text{trans}}, \mathcal{I}_{\text{req}}^{\text{trans}}$ and rotational parts $\mathcal{I}_{\text{robot}}^{\text{orien}}, \mathcal{I}_{\text{req}}^{\text{orien}}$, where the translational ones contain the x and y states and the orientational ones contain the yaw state.

The skill is further divided into translational and rotational skills. A translational skill $o_{\text{trans}} \in \mathcal{O}_{\text{trans}}$ consists of sets of preconditions $\Sigma_{o_{\text{trans}}}^{\text{pre}} \subseteq \Sigma_{\text{robot}} \times \Sigma_{\text{terrain}}$ that include the full robot state, and translational-only postconditions $\Sigma_{o_{\text{trans}}}^{\text{post}} \subseteq \Sigma_{\text{robot}}^{\text{trans}}$. A rotational skill in place $o_{\text{orien}} \in \mathcal{O}_{\text{orien}}$ consists of sets of rotational-only preconditions $\Sigma_{o_{\text{orien}}}^{\text{pre}} \subseteq \Sigma_{\text{robot}}^{\text{orien}}$ and postconditions $\Sigma_{o_{\text{orien}}}^{\text{post}} \subseteq \Sigma_{\text{robot}}^{\text{orien}}$. The terrain state can also be incorporated when generating rotational skills, particularly for terrains that pose challenges for turning. However, we omit this in our current implementation for simplicity. The specification encoding then follows the same procedure as described in Sec. VI-B, based on each skill's precondition and postcondition. The hard constraints remain unchanged, except that translational and rotational ones are defined separately to ensure the corresponding states remain unchanged when no skill is selected.

To demonstrate the resulting maneuver, we construct a scenario with multiple dense and sparse stepping stones arranged in an overall zig-zag pattern, requiring several turning behaviors. Although sideways movement skills are feasible, we manually exclude them before synthesis to highlight yaw adjustments controlled by the rotational skills. As shown in Fig. 12, the robot executes multiple turns to continuously progress towards the global waypoint. More complex coupled translational and rotational behaviors can also be defined by modifying the preconditions and postconditions associated with each skill.

X. Hardware Demonstrations

We demonstrate that our entire framework can be successfully deployed on hardware, highlighting two key aspects. First, we showcase the framework's capability to generate adaptive locomotion gaits across diverse terrain types, particularly focusing on agile leaping motions. Second, we illustrate the framework's assured safety through obstacle avoidance and selection of dynamically feasible gaits, benchmarked against a heuristic-based planner.

A. Hardware Experiment Setup

For hardware experiments, we set up similar real-world scenarios for both unstructured and rebar terrains. For the unstructured terrain scenario, we construct wooden blocks to form stepping stones, gaps, and flat regions, with each stepping

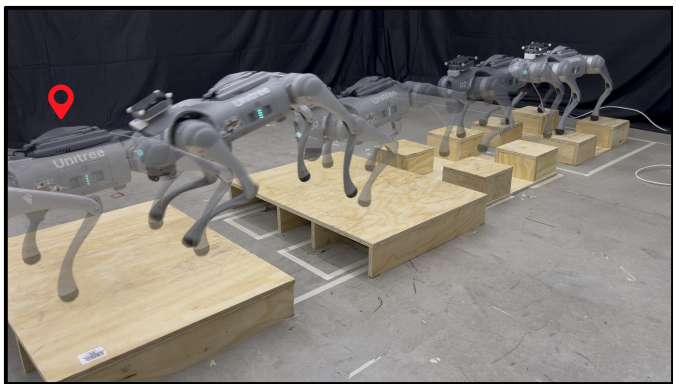

Fig. 14. Hardware experiment demonstration for the second unstructured terrain scenario with sparse stepping stones, flat, and gap terrains.

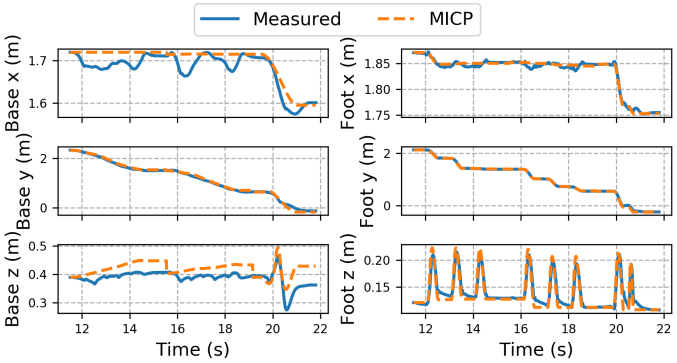

Fig. 15. Task-space tracking of the base and front-left foot positions: comparison between measured states and MICP-generated reference trajectories.

stone elevated approximately 0.12 m above the ground. For the rebar scenario, we assemble a realistic rebar mat using fourteen $1/2$-inch $\times$ 4-foot rebars and six $1/2$-inch $\times$ 10-foot rebars. In the synthesis setup, obstacles are considered a distinct terrain type, consistent with the simulation. Both scenarios assume the maximum potential terrain types—8 for unstructured and 14 for rebar—though the real setups include fewer types. As demonstrated in the simulation, this does not increase complexity, as it only scales linearly with terrain-request pairs due to our high-level manager. For safety, we set abstraction cell sizes to 0.8 m for the unstructured terrain and 0.45 m for the rebar terrain.

B. Unstructured Terrain

As shown in Fig. 13, we first create a scenario with sparse stepping stones and flat terrain regions. The stepping stones are spaced between $0.18-0.23$ m apart. Both side and front views are provided to highlight the misalignment of stepping stones along the robot walking direction. **Ye: [check if this change makes sense]Ziyi: [LGTM]**he MICP planner successfully generates a reference trajectory involving non-trivial sideways movement, enabling the robot to safely land on the stepping stones. All transitions utilize a 3 s trotting gait.

In the second scenario, shown in Fig. 14, we further include a gap terrain segment. The gap, approximately 30 cm wide, necessitates the use of a leaping gait. Since the gap terrain was incorporated during offline synthesis, our framework can directly select an optimized 1.5 s leaping gait generated by gait-free MICP upon encountering this gap terrain. The task-space tracking performance between the measured state and the reference trajectory generated by the online MICP is shown in Fig. 15. This includes the floating base position and the end-effector (EE) position for the front-left foot. The EE tracking maintains errors within 0.01 m in the x and y axes, ensuring precise foot placement. Meanwhile, the NMPC effectively adjusts the base position to compensate for model simplifications at the MICP level, enabling successful execution of both trotting and leaping motions.

C. Rebar Terrain

For the rebar terrain scenarios shown in Fig. 16, we test two cases: one without any obstacles and one with an obstacle introduced during execution. The rebar spacing varies between 0.1 m and 0.3 m. Offline synthesis is conducted without prior knowledge of obstacles. In the first case (top row), the robot Chotu successfully performs the entire maneuver without encountering any runtime failures, consistently moving forward until reaching the goal waypoint. In the second case (bottom row), an obstacle is added to the environment but only detected during the online execution phase. Upon encountering a new terrain/request pair caused by the obstacle, the planner promptly triggers a runtime resynthesis. Leveraging previously generated skills, it computes a new strategy within 0.05 s to detour around the obstacle and continue toward the goal. All transitions in both scenarios use a 2.25 s static walking gait, where only one foot is lifted at a time to ensure safety.

D. Benchmark: Heuristics-Based Planner

We create a third rebar scenario, shown in Fig. 17, by removing two rebars to further increase the maximum spacing to 0.48 m. This highlights the safety advantage of our planner compared to a heuristics-based footstep planner. The heuristic baseline follows a similar strategy to [4], [7], adapted for the rebar scenario by selecting the nearest rebar polygon and the closest feasible foothold to a nominal target. The resulting footstep plan and linearly interpolated base trajectory are sent to the same tracking control module. For fairness, all parameters are tuned to achieve successful traversal at a speed of 0.1 m/s (as shown in the supplemental video).

Without re-performing the offline synthesis, our framework directly uses the results from Sec. X-C. It classifies the extreme sparse region as an obstacle and performs runtime resynthesis, generating a detour to safely reach the goal. In contrast, we task the heuristics-based planner with the same goal at 0.2 m/s to match our planner's effective gait speed (i.e., 0.45 m per 2.25 s transition). Without reasoning about the compatibility between terrain geometry and gait feasibility, the heuristic planner suffers from poor EE tracking after a few steps, leading to foot slippage and eventual failure as the robot is entangled by the sparse rebar layout.

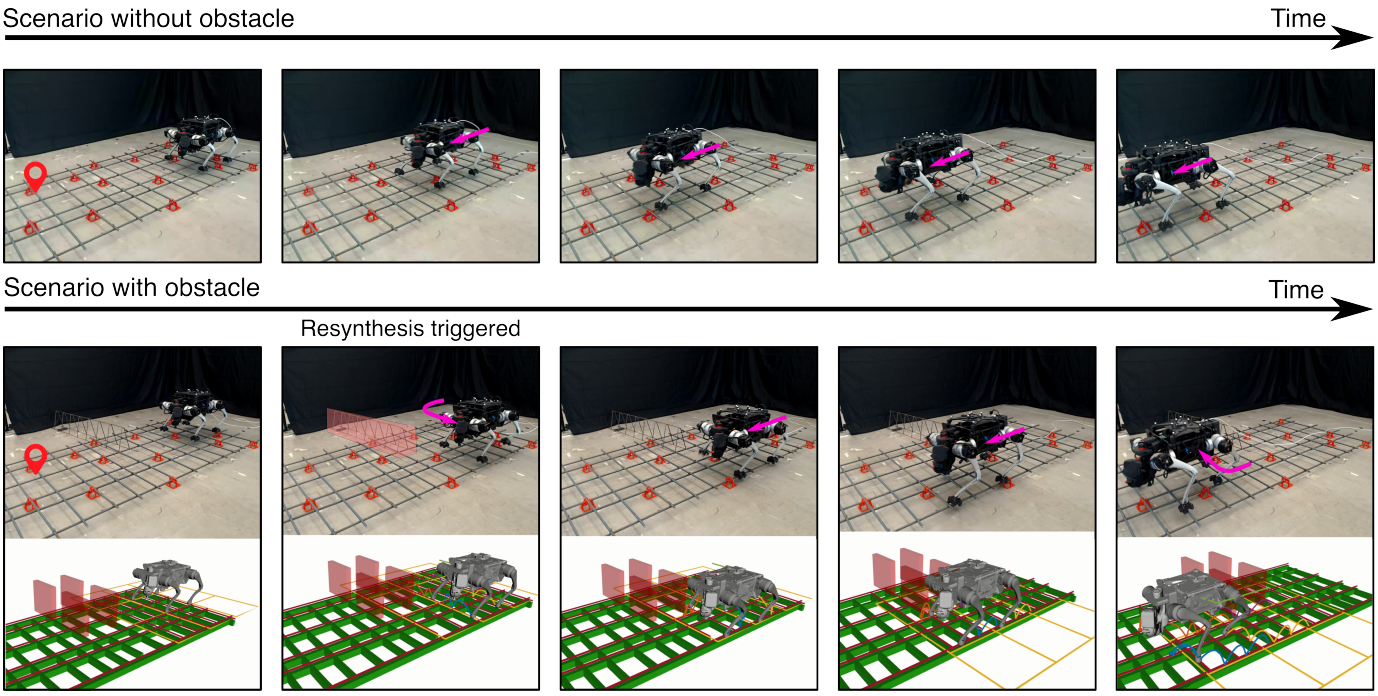

Fig. 16. Execution results in rebar terrain without (top row) and with obstacle (bottom row). In the obstacle case, runtime resynthesis is triggered to generate a detour strategy and ensure successful traversal.

TABLE V
ONLINE GAIT-FIXED MICP SOLVING TIME FOR HARDWARE

Scenario	Polygons	Min (s)	Mean (s)	Max (s)
Unstructured - Scene 1	6	0.81	4.04	7.86
Unstructured - Scene 2	5	0.16	0.53	0.96
Rebar - Scene 1	8	3.88	6.54	9.26
Rebar - Scene 2	7.5	3.60	9.13	19.23
Rebar - Scene 3	6.33	2.45	7.37	14.7

E. Computational Time

We report the hardware computational time in Table V. Except for the second scenario in the unstructured terrain, we observe a notable increase in solve time compared to simulation. This is mainly due to two factors: (1) In the first unstructured terrain scenario, the two sets of stepping stones are laterally misaligned from the robot's viewpoint, requiring non-trivial deviation from the nominal foot location and sideways movement; **Ye: [Does the robot really have a sideway move? It is bit hard to tell in the video.]Ziyi: [I rephrased it.]**2) In the rebar scenarios, the real-world rebar polygons are not perfectly aligned with the x or y-axis as in simulation, introducing additional numerical complexity for branch-and-bound solvers. Further acceleration of MIP solving through tighter convex relaxations [96], [97] remains an important direction for future work.

XI. DISCUSSION

A. Generalization to More Types of Terrain

The current framework relies on manual terrain abstraction and classification, which requires expert knowledge to define terrain types and assign them to discrete symbolic categories. This process typically involves analyzing physical features such as terrain shape, height variation, and support area to determine whether a terrain segment should be labeled as flat, sparse, dense, high, gap, etc. While effective, this expert-driven approach may limit scalability and generalization to novel environments or terrain conditions. Future extensions could incorporate data-driven terrain classification and generation methods, such as supervised learning or clustering based on 3D point cloud statistics to automate the terrain abstraction process and reduce reliance on human heuristics.

B. Perception Module

The proposed framework is modular and can be directly integrated with a wide range of perception pipelines that provide terrain geometry in the form of segmented polygonal regions [98]. Existing perception modules that perform terrain segmentation using LiDAR, RGB-D sensors, or stereo vision can be adapted to supply the required input to the MICP planner and symbolic abstraction layers.

XII. CONCLUSION

In this work, we presented an integrated planning framework for terrain-adaptive locomotion that combines reactive synthesis with MICP, enabling safe and reactive responses in dynamically changing environments. To address unrealizable specifications arising from limited motion primitives, we introduced a symbolic repair approach that incorporates dynamic feasibility checks, automatically identifying missing transitions necessary for navigating adversarial terrains. In

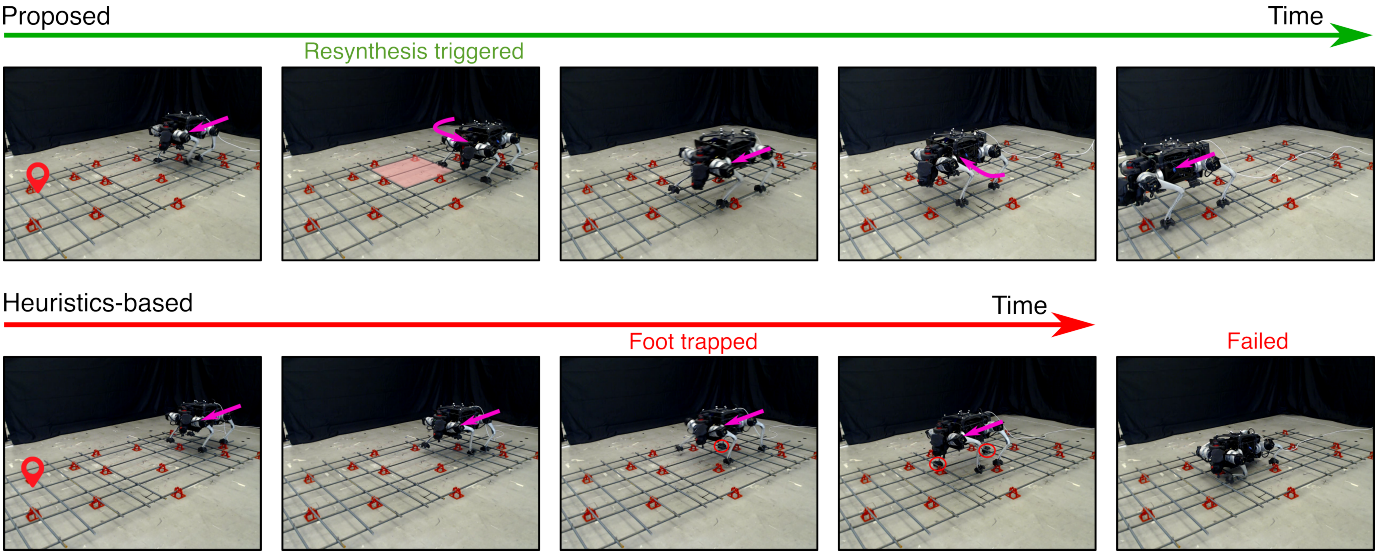

Fig. 17. Comparison between the proposed method and a heuristics-based planner in an extreme sparse rebar scenario. The proposed method performs resynthesis and succeeds, while the heuristics-based planner fails due to foot trapping.

the online execution phase, we tackled the disparity between offline synthesis and real-world conditions by using an online MICP solver and a runtime repair process based on real-world terrain data, including unforeseen terrain conditions. Our approach not only enhances motion feasibility and safety but also provides a scalable solution for legged robots maneuvering in complex and safety-critical environments.

XIII. Acknowledgment

We thank Eohan George and Suphakorn Lertruchtkul for their hardware support on Chotu and contributions to rebar scenario design, and Pengyuan Shu for constructing the real-world terrains.

References

[1] J. Di Carlo, P. M. Wensing, B. Katz, G. Bledt, and S. Kim, "Dynamic locomotion in the mit cheetah 3 through convex model-predictive control," in *2018 IEEE/RSJ international conference on intelligent robots and systems (IROS)*. IEEE, 2018, pp. 1–9.

[2] D. Kim, J. Di Carlo, B. Katz, G. Bledt, and S. Kim, "Highly dynamic quadruped locomotion via whole-body impulse control and model predictive control," *arXiv preprint arXiv:1909.06586*, 2019.

[3] Z. Zhou, B. Wingo, N. Boyd, S. Hutchinson, and Y. Zhao, "Momentum-aware trajectory optimization and control for agile quadrupedal locomotion," *IEEE Robotics and Automation Letters*, vol. 7, no. 3, pp. 7755–7762, 2022.

[4] P. Fankhauser, M. Bjelonic, C. D. Bellicoso, T. Miki, and M. Hutter, "Robust rough-terrain locomotion with a quadrupedal robot," in *2018 IEEE International Conference on Robotics and Automation (ICRA)*. IEEE, 2018, pp. 5761–5768.

[5] R. Grandia, F. Jenelten, S. Yang, F. Farshidian, and M. Hutter, "Perceptive locomotion through nonlinear model-predictive control," *IEEE Transactions on Robotics*, 2023.

[6] H.-W. Park, P. M. Wensing, and S. Kim, "Online planning for autonomous running jumps over obstacles in high-speed quadrupeds," in *Robotics: Science and Systems*, 2015.

[7] D. Kim, D. Carballo, J. Di Carlo, B. Katz, G. Bledt, B. Lim, and S. Kim, "Vision aided dynamic exploration of unstructured terrain with a small-scale quadruped robot," in *IEEE International Conference on Robotics and Automation*. IEEE, 2020, pp. 2464–2470.

[8] S. Gilroy, D. Lau, L. Yang, E. Izaguirre, K. Biermayer, A. Xiao, M. Sun, A. Agrawal, J. Zeng, Z. Li *et al.*, "Autonomous navigation for quadrupedal robots with optimized jumping through constrained obstacles," in *2021 IEEE 17th International Conference on Automation Science and Engineering (CASE)*. IEEE, 2021, pp. 2132–2139.

[9] J. Norby and A. M. Johnson, "Fast global motion planning for dynamic legged robots," in *2020 IEEE/RSJ International Conference on Intelligent Robots and Systems*. IEEE, 2020, pp. 3829–3836.

[10] M. Chignoli, S. Morozov, and S. Kim, "Rapid and reliable quadruped motion planning with omnidirectional jumping," in *International Conference on Robotics and Automation*. IEEE, 2022, pp. 6621–6627.

[11] Y. Zhao, Y. Li, L. Sentis, U. Topcu, and J. Liu, "Reactive task and motion planning for robust whole-body dynamic locomotion in constrained environments," *The International Journal of Robotics Research*, p. 02783649221077714, 2022.

[12] A. Shamsah, Z. Gu, J. Warnke, S. Hutchinson, and Y. Zhao, "Integrated task and motion planning for safe legged navigation in partially observable environments," *IEEE Transactions on Robotics*, 2023.

[13] A. K. Valenzuela, "Mixed-integer convex optimization for planning aggressive motions of legged robots over rough terrain," Ph.D. dissertation, Massachusetts Institute of Technology, 2016.

[14] Y. Shirai, X. Lin, A. Schperberg, Y. Tanaka, H. Kato, V. Vichathorn, and D. Hong, "Simultaneous contact-rich grasping and locomotion via distributed optimization enabling free-climbing for multi-limbed robots," in *2022 IEEE/RSJ International Conference on Intelligent Robots and Systems (IROS)*. IEEE, 2022, pp. 13 563–13 570.

[15] R. Deits and R. Tedrake, "Footstep planning on uneven terrain with mixed-integer convex optimization," in *2014 IEEE-RAS international conference on humanoid robots*. IEEE, 2014, pp. 279–286.

[16] H. Dai, G. Izatt, and R. Tedrake, "Global inverse kinematics via mixed-integer convex optimization," *The International Journal of Robotics Research*, vol. 38, no. 12-13, pp. 1420–1441, 2019.

[17] Y. Ding, C. Li, and H.-W. Park, "Kinodynamic motion planning for multi-legged robot jumping via mixed-integer convex program," in *2020 IEEE/RSJ International Conference on Intelligent Robots and Systems (IROS)*. IEEE, 2020, pp. 3998–4005.

[18] N. Fey, R. J. Frei, and P. M. Wensing, "3d hopping in discontinuous terrain using impulse planning with mixed-integer strategies," *IEEE Robotics and Automation Letters*, 2024.

[19] B. Ponton, A. Herzog, S. Schaal, and L. Righetti, "A convex model of humanoid momentum dynamics for multi-contact motion generation," in *2016 IEEE-RAS 16th International Conference on Humanoid Robots (Humanoids)*. IEEE, 2016, pp. 842–849.

[20] F. Risbourg, T. Corbères, P.-A. Léziart, T. Flayols, N. Mansard, and S. Tonneau, "Real-time footstep planning and control of the solo

quadruped robot in 3d environments," in *IEEE/RSJ International Conference on Intelligent Robots and Systems*, 2022, pp. 12 950–12 956.
[21] B. Acosta and M. Posa, "Bipedal walking on constrained footholds with mpc footstep control," in *2023 IEEE-RAS 22nd International Conference on Humanoid Robots*. IEEE, 2023, pp. 1–8.
[22] B. Aceituno-Cabezas, C. Mastalli, H. Dai, M. Focchi, A. Radulescu, D. G. Caldwell, J. Cappelletto, J. C. Grieco, G. Fernández-López, and C. Semini, "Simultaneous contact, gait, and motion planning for robust multilegged locomotion via mixed-integer convex optimization," *IEEE Robotics and Automation Letters*, vol. 3, no. 3, pp. 2531–2538, 2017.
[23] R. Bloem, B. Jobstmann, N. Piterman, A. Pnueli, and Y. Saar, "Synthesis of reactive (1) designs," *Journal of Computer and System Sciences*, vol. 78, no. 3, pp. 911–938, 2012.
[24] M. Wermelinger, P. Fankhauser, R. Diethelm, P. Krüsi, R. Siegwart, and M. Hutter, "Navigation planning for legged robots in challenging terrain," in *2016 IEEE/RSJ International Conference on Intelligent Robots and Systems (IROS)*. IEEE, 2016, pp. 1184–1189.
[25] P. Fernbach, S. Tonneau, A. Del Prete, and M. Taïx, "A kinodynamic steering-method for legged multi-contact locomotion," in *2017 IEEE/RSJ International Conference on Intelligent Robots and Systems (IROS)*. IEEE, 2017, pp. 3701–3707.
[26] Q. Liao, Z. Li, A. Thirugnanam, J. Zeng, and K. Sreenath, "Walking in narrow spaces: Safety-critical locomotion control for quadrupedal robots with duality-based optimization," in *2023 IEEE/RSJ International Conference on Intelligent Robots and Systems (IROS)*. IEEE, 2023, pp. 2723–2730.
[27] S. Feng, Z. Zhou, J. S. Smith, M. Asselmeier, Y. Zhao, and P. A. Vela, "Gpf-bg: A hierarchical vision-based planning framework for safe quadrupedal navigation," in *2023 IEEE International Conference on Robotics and Automation (ICRA)*. IEEE, 2023, pp. 1968–1975.
[28] A. Pacheck and H. Kress-Gazit, "Physically feasible repair of reactive, linear temporal logic-based, high-level tasks," *IEEE Transactions on Robotics*, 2023.
[29] Q. Meng and H. Kress-Gazit, "Automated Robot Recovery from Assumption Violations of High-Level Specifications," in *2024 IEEE 20th International Conference on Automation Science and Engineering (CASE)*. IEEE, Aug. 2024, pp. 4154–4161.
[30] J. Z. Kolter, M. P. Rodgers, and A. Y. Ng, "A control architecture for quadruped locomotion over rough terrain," in *2008 IEEE International Conference on Robotics and Automation*. IEEE, 2008, pp. 811–818.
[31] M. Kalakrishnan, J. Buchli, P. Pastor, M. Mistry, and S. Schaal, "Fast, robust quadruped locomotion over challenging terrain," in *2010 IEEE International Conference on Robotics and Automation*. IEEE, 2010, pp. 2665–2670.
[32] A. Winkler, I. Havoutis, S. Bazeille, J. Ortiz, M. Focchi, R. Dillmann, D. Caldwell, and C. Semini, "Path planning with force-based foothold adaptation and virtual model control for torque controlled quadruped robots," in *2014 IEEE International Conference on Robotics and Automation (ICRA)*. IEEE, 2014, pp. 6476–6482.
[33] C. Mastalli, I. Havoutis, A. W. Winkler, D. G. Caldwell, and C. Semini, "On-line and on-board planning and perception for quadrupedal locomotion," in *2015 IEEE International Conference on Technologies for Practical Robot Applications (TePRA)*. IEEE, 2015, pp. 1–7.
[34] R. J. Griffin, G. Wiedebach, S. McCrory, S. Bertrand, I. Lee, and J. Pratt, "Footstep planning for autonomous walking over rough terrain," in *2019 IEEE-RAS 19th international conference on humanoid robots (humanoids)*. IEEE, 2019, pp. 9–16.
[35] S. Tonneau, D. Song, P. Fernbach, N. Mansard, M. Taïx, and A. Del Prete, "Sl1m: Sparse l1-norm minimization for contact planning on uneven terrain," in *2020 IEEE International Conference on Robotics and Automation (ICRA)*. IEEE, 2020, pp. 6604–6610.
[36] K. Hauser, T. Bretl, and J.-C. Latombe, "Non-gaited humanoid locomotion planning," in *5th IEEE-RAS International Conference on Humanoid Robots, 2005.* IEEE, 2005, pp. 7–12.
[37] T. Bretl, "Motion planning of multi-limbed robots subject to equilibrium constraints: The free-climbing robot problem," *The International Journal of Robotics Research*, vol. 25, no. 4, pp. 317–342, 2006.
[38] S. Tonneau, A. Del Prete, J. Pettré, C. Park, D. Manocha, and N. Mansard, "An efficient acyclic contact planner for multiped robots," *IEEE Transactions on Robotics*, vol. 34, no. 3, pp. 586–601, 2018.
[39] F. Jenelten, T. Miki, A. E. Vijayan, M. Bjelonic, and M. Hutter, "Perceptive locomotion in rough terrain–online foothold optimization," *IEEE Robotics and Automation Letters*, vol. 5, no. 4, pp. 5370–5376, 2020.
[40] A. Agrawal, S. Chen, A. Rai, and K. Sreenath, "Vision-aided dynamic quadrupedal locomotion on discrete terrain using motion libraries," in *2022 International Conference on Robotics and Automation (ICRA)*. IEEE, 2022, pp. 4708–4714.
[41] O. A. V. Magana, V. Barasuol, M. Camurri, L. Franceschi, M. Focchi, M. Pontil, D. G. Caldwell, and C. Semini, "Fast and continuous foothold adaptation for dynamic locomotion through cnns," *IEEE Robotics and Automation Letters*, vol. 4, no. 2, pp. 2140–2147, 2019.
[42] O. Villarreal, V. Barasuol, P. M. Wensing, D. G. Caldwell, and C. Semini, "Mpc-based controller with terrain insight for dynamic legged locomotion," in *2020 IEEE International Conference on Robotics and Automation (ICRA)*. IEEE, 2020, pp. 2436–2442.
[43] W. Yu, D. Jain, A. Escontrela, A. Iscen, P. Xu, E. Coumans, S. Ha, J. Tan, and T. Zhang, "Visual-locomotion: Learning to walk on complex terrains with vision," in *5th Annual Conference on Robot Learning*, 2021.
[44] S. Gangapurwala, M. Geisert, R. Orsolino, M. Fallon, and I. Havoutis, "Rloc: Terrain-aware legged locomotion using reinforcement learning and optimal control," *IEEE Transactions on Robotics*, vol. 38, no. 5, pp. 2908–2927, 2022.
[45] R. Grandia, A. J. Taylor, A. D. Ames, and M. Hutter, "Multi-layered safety for legged robots via control barrier functions and model predictive control," in *2021 IEEE International Conference on Robotics and Automation (ICRA)*. IEEE, 2021, pp. 8352–8358.
[46] F. Jenelten, R. Grandia, F. Farshidian, and M. Hutter, "Tamols: Terrain-aware motion optimization for legged systems," *IEEE Transactions on Robotics*, vol. 38, no. 6, pp. 3395–3413, 2022.
[47] X. Da, Z. Xie, D. Hoeller, B. Boots, A. Anandkumar, Y. Zhu, B. Babich, and A. Garg, "Learning a contact-adaptive controller for robust, efficient legged locomotion," in *Conference on Robot Learning*. PMLR, 2021, pp. 883–894.
[48] Y. Yang, T. Zhang, E. Coumans, J. Tan, and B. Boots, "Fast and efficient locomotion via learned gait transitions," in *Conference on Robot Learning*. PMLR, 2022, pp. 773–783.
[49] Z. Xie, X. Da, B. Babich, A. Garg, and M. v. de Panne, "Glide: Generalizable quadrupedal locomotion in diverse environments with a centroidal model," in *International Workshop on the Algorithmic Foundations of Robotics*. Springer, 2022, pp. 523–539.
[50] G. B. Margolis, T. Chen, K. Paigwar, X. Fu, D. Kim, S. b. Kim, and P. Agrawal, "Learning to jump from pixels," in *Proceedings of the 5th Conference on Robot Learning*. PMLR, 2022, pp. 1025–1034.
[51] S. Yu, N. Perera, D. Marew, and D. Kim, "Learning generic and dynamic locomotion of humanoids across discrete terrains," *arXiv preprint arXiv:2405.17227*, 2024.
[52] C. Boussema, M. J. Powell, G. Bledt, A. J. Ijspeert, P. M. Wensing, and S. Kim, "Online gait transitions and disturbance recovery for legged robots via the feasible impulse set," *IEEE Robotics and automation letters*, vol. 4, no. 2, pp. 1611–1618, 2019.
[53] K. Wang, Z. J. Hu, P. Tisnikar, O. Helander, D. Chappell, and P. Kormushev, "When and where to step: Terrain-aware real-time footstep location and timing optimization for bipedal robots," *arXiv preprint arXiv:2302.07345*, 2023.
[54] H. Sun, J. Yang, Y. Jia, and C. Wang, "Free gait generation of quadruped robots via impulse-based feasibility analysis," *IEEE/ASME Transactions on Mechatronics*, 2023.
[55] M. Posa, C. Cantu, and R. Tedrake, "A direct method for trajectory optimization of rigid bodies through contact," *The International Journal of Robotics Research*, vol. 33, no. 1, pp. 69–81, 2014.
[56] I. Mordatch, E. Todorov, and Z. Popović, "Discovery of complex behaviors through contact-invariant optimization," *ACM Transactions on Graphics (ToG)*, vol. 31, no. 4, pp. 1–8, 2012.
[57] A. Aydinoglu and M. Posa, "Real-time multi-contact model predictive control via admm," in *2022 International Conference on Robotics and Automation (ICRA)*. IEEE, 2022, pp. 3414–3421.
[58] S. Le Cleac'h, T. A. Howell, S. Yang, C.-Y. Lee, J. Zhang, A. Bishop, M. Schwager, and Z. Manchester, "Fast contact-implicit model predictive control," *IEEE Transactions on Robotics*, 2024.
[59] X. Jiang, W. Chi, Y. Zheng, S. Zhang, Y. Ling, J. Xu, and Z. Zhang, "Locomotion generation for quadruped robots on challenging terrains via quadratic programming," *Autonomous Robots*, vol. 47, no. 1, pp. 51–76, 2023.
[60] C. R. Garrett, R. Chitnis, R. Holladay, B. Kim, T. Silver, L. P. Kaelbling, and T. Lozano-Pérez, "Integrated task and motion planning," *Annual review of control, robotics, and autonomous systems*, vol. 4, no. 1, pp. 265–293, 2021.

[61] M. Toussaint, "Logic-geometric programming: An optimization-based approach to combined task and motion planning." in *IJCAI*, 2015, pp. 1930–1936.

[62] M. A. Toussaint, K. R. Allen, K. A. Smith, and J. B. Tenenbaum, "Differentiable physics and stable modes for tool-use and manipulation planning," 2018.

[63] T. Migimatsu and J. Bohg, "Object-centric task and motion planning in dynamic environments," *IEEE Robotics and Automation Letters*, vol. 5, no. 2, pp. 844–851, 2020.

[64] Z. Zhao, Z. Zhou, M. Park, and Y. Zhao, "Sydebo: Symbolic-decision-embedded bilevel optimization for long-horizon manipulation in dynamic environments," *IEEE Access*, vol. 9, pp. 128 817–128 826, 2021.

[65] J.-P. Sleiman, F. Farshidian, and M. Hutter, "Versatile multicontact planning and control for legged loco-manipulation," *Science Robotics*, vol. 8, no. 81, p. eadg5014, 2023.

[66] Y. Ding, M. Zhang, C. Li, H.-W. Park, and K. Hauser, "Hybrid sampling/optimization-based planning for agile jumping robots on challenging terrains," in *2021 IEEE International Conference on Robotics and Automation (ICRA)*. IEEE, 2021, pp. 2839–2845.

[67] Y. Shirai, X. Lin, A. Mehta, and D. Hong, "Lto: lazy trajectory optimization with graph-search planning for high dof robots in cluttered environments," in *2021 IEEE International Conference on Robotics and Automation (ICRA)*. IEEE, 2021, pp. 7533–7539.

[68] E. Jelavic, F. Farshidian, and M. Hutter, "Combined sampling and optimization based planning for legged-wheeled robots," in *2021 IEEE International Conference on Robotics and Automation (ICRA)*. IEEE, 2021, pp. 8366–8372.

[69] L. Amatucci, J.-H. Kim, J. Hwangbo, and H.-W. Park, "Monte carlo tree search gait planner for non-gaited legged system control," in *2022 International Conference on Robotics and Automation (ICRA)*. IEEE, 2022, pp. 4701–4707.

[70] C. Chen, P. Culbertson, M. Lepert, M. Schwager, and J. Bohg, "Trajectotree: Trajectory optimization meets tree search for planning multi-contact dexterous manipulation," in *2021 IEEE/RSJ International Conference on Intelligent Robots and Systems (IROS)*. IEEE, 2021, pp. 8262–8268.

[71] M. Zhang, D. K. Jha, A. U. Raghunathan, and K. Hauser, "Simultaneous trajectory optimization and contact selection for multi-modal manipulation planning," *arXiv preprint arXiv:2306.06465*, 2023.

[72] H. Zhu, A. Meduri, and L. Righetti, "Efficient object manipulation planning with monte carlo tree search," in *2023 IEEE/RSJ International Conference on Intelligent Robots and Systems (IROS)*. IEEE, 2023, pp. 10 628–10 635.

[73] M. Asselmeier, J. Ivanova, Z. Zhou, P. A. Vela, and Y. Zhao, "Hierarchical experience-informed navigation for multi-modal quadrupedal rebar grid traversal," in *2024 IEEE International Conference on Robotics and Automation (ICRA)*. IEEE, 2024, pp. 8065–8072.

[74] H. Kress-Gazit, M. Lahijanian, and V. Raman, "Synthesis for robots: Guarantees and feedback for robot behavior," *Annual Review of Control, Robotics, and Autonomous Systems*, vol. 1, pp. 211–236, 2018.

[75] S. Kulgod, W. Chen, J. Huang, Y. Zhao, and N. Atanasov, "Temporal logic guided locomotion planning and control in cluttered environments," in *American Control Conference*. IEEE, 2020, pp. 5425–5432.

[76] Z. Zhou, D. J. Lee, Y. Yoshinaga, S. Balakirsky, D. Guo, and Y. Zhao, "Reactive task allocation and planning for quadrupedal and wheeled robot teaming," in *IEEE International Conference on Automation Science and Engineering*. IEEE, 2022, pp. 2110–2117.

[77] J. Jiang, S. Coogan, and Y. Zhao, "Abstraction-based planning for uncertainty-aware legged navigation," *IEEE Open Journal of Control Systems*, 2023.

[78] Z. Gu, N. Boyd, and Y. Zhao, "Reactive locomotion decision-making and robust motion planning for real-time perturbation recovery," in *2022 International Conference on Robotics and Automation (ICRA)*. IEEE, 2022, pp. 1896–1902.

[79] A. Pnueli and R. Rosner, "On the synthesis of a reactive module," in *Proceedings of the 16th ACM SIGPLAN-SIGACT symposium on Principles of programming languages*, 1989, pp. 179–190.

[80] H. Kress-Gazit, G. E. Fainekos, and G. J. Pappas, "Temporal-logic-based reactive mission and motion planning," *IEEE transactions on robotics*, vol. 25, no. 6, pp. 1370–1381, 2009.

[81] J. A. DeCastro, R. Ehlers, M. Rungger, A. Balkan, P. Tabuada, and H. Kress-Gazit, "Dynamics-based reactive synthesis and automated revisions for high-level robot control," *arXiv preprint arXiv:1410.6375*, 2014.

[82] G. E. Fainekos, S. G. Loizou, and G. J. Pappas, "Translating temporal logic to controller specifications," in *Proceedings of the 45th IEEE Conference on Decision and Control*. IEEE, 2006, pp. 899–904.

[83] A. Bhatia, L. E. Kavraki, and M. Y. Vardi, "Sampling-based motion planning with temporal goals," in *2010 IEEE International Conference on Robotics and Automation*. IEEE, 2010, pp. 2689–2696.

[84] J. Liu, N. Ozay, U. Topcu, and R. M. Murray, "Synthesis of reactive switching protocols from temporal logic specifications," *IEEE Transactions on Automatic Control*, vol. 58, no. 7, pp. 1771–1785, 2013.

[85] M. R. Maly, M. Lahijanian, L. E. Kavraki, H. Kress-Gazit, and M. Y. Vardi, "Iterative temporal motion planning for hybrid systems in partially unknown environments," in *Proceedings of the 16th international conference on Hybrid systems: computation and control*, 2013, pp. 353–362.

[86] A. Pacheck, S. Moarref, and H. Kress-Gazit, "Finding missing skills for high-level behaviors," in *2020 IEEE International Conference on Robotics and Automation (ICRA)*. IEEE, 2020, pp. 10 335–10 341.

[87] R. Ehlers and V. Raman, "Slugs: Extensible GR(1) synthesis," in *International Conference on Computer Aided Verification*. Springer, 2016, pp. 333–339.

[88] C. Baier and J.-P. Katoen, *Principles of model checking*. MIT press, 2008.

[89] H. Dai, A. Valenzuela, and R. Tedrake, "Whole-body motion planning with centroidal dynamics and full kinematics," in *2014 IEEE-RAS International Conference on Humanoid Robots*. IEEE, 2014, pp. 295–302.

[90] M. Chignoli, D. Kim, E. Stanger-Jones, and S. Kim, "The mit humanoid robot: Design, motion planning, and control for acrobatic behaviors," in *2020 IEEE-RAS 20th International Conference on Humanoid Robots (Humanoids)*. IEEE, 2021, pp. 1–8.

[91] J.-P. Sleiman, F. Farshidian, M. V. Minniti, and M. Hutter, "A unified mpc framework for whole-body dynamic locomotion and manipulation," *IEEE Robotics and Automation Letters*, vol. 6, no. 3, pp. 4688–4695, 2021.

[92] F. Farshidian *et al.*, "OCS2: An open source library for optimal control of switched systems," [Online]. Available: https://github.com/leggedrobotics/ocs2.

[93] S. Kuindersma, F. Permenter, and R. Tedrake, "An efficiently solvable quadratic program for stabilizing dynamic locomotion," in *2014 IEEE International Conference on Robotics and Automation (ICRA)*. IEEE, 2014, pp. 2589–2594.

[94] P. M. Wensing and D. E. Orin, "Generation of dynamic humanoid behaviors through task-space control with conic optimization," in *2013 IEEE International Conference on Robotics and Automation*. IEEE, 2013, pp. 3103–3109.

[95] G. Bledt, M. J. Powell, B. Katz, J. Di Carlo, P. M. Wensing, and S. Kim, "Mit cheetah 3: Design and control of a robust, dynamic quadruped robot," in *2018 IEEE/RSJ International Conference on Intelligent Robots and Systems (IROS)*. IEEE, 2018, pp. 2245–2252.

[96] T. Marcucci, J. Umenberger, P. Parrilo, and R. Tedrake, "Shortest paths in graphs of convex sets," *SIAM Journal on Optimization*, vol. 34, no. 1, pp. 507–532, 2024.

[97] X. Lin, "Accelerate hybrid model predictive control using generalized benders decomposition," *arXiv preprint arXiv:2406.00780*, 2024.

[98] T. Miki, L. Wellhausen, R. Grandia, F. Jenelten, T. Homberger, and M. Hutter, "Elevation mapping for locomotion and navigation using gpu," in *2022 IEEE/RSJ International Conference on Intelligent Robots and Systems (IROS)*. IEEE, 2022, pp. 2273–2280.